7-10-2006

Study of Upward-Facing Spray Cooling with Water at Atmospheric Pressure

Alberto D. Sato
University of South Florida

Study of Upward-Facing Spray Cooling with Water at Atmospheric Pressure

by

Alberto D. Sato

A thesis submitted in partial fulfillment
of the requirements for the degree of
Master of Science in Mechanical Engineering
Department of Mechanical Engineering
College of Engineering
University of South Florida

Major Professor: Frank Pyrtle, III, Ph.D.
Muhammad Mustafizur Rahman, Ph.D.
Craig Lusk, Ph.D.

Date of Approval:
July 10, 2006

Keywords: heat transfer, conduction, steady-state, heat flux, heated surface

Dedication

To

My Family

Without them I would not be able to complete this thesis

To

My Advisor Professor Frank Pyrtle III

Thanks for your guidance

Thanks a Lot

Table of Contents

List of Tables iii

List of Figures iv

List of Symbols vii

Abstract x

Chapter 1 – Background 1
- 1.1 Literature Review 2
- 1.2 Heat Transfer Regimes 23
- 1.3 Objectives of the Present Study 26
- 1.4 Determination of Heat Flux and Surface Temperature 26
- 1.5 Determination of Heat Transfer Coefficient 29
- 1.6 Uncertainty and Error Analysis 30

Chapter 2 - Experimental Methods and Procedures 33
- 2.1 Experimental Apparatus 34
  - 2.1.1 Fluid System 34
  - 2.1.2 Heater System 36
  - 2.1.3 Acquisition System 39
- 2.2 Operating Procedure 42
- 2.3 Experimental Parameters 44
  - 2.3.1 Distance between Test Surface and Nozzle 44
  - 2.3.2 Volumetric Flow Rate 46

Chapter 3 - Experimental Results 47
- 3.1 Heat Flux and Temperature of Surface Calculation 47
- 3.2 Heat Transfer Coefficient Calculation 47
- 3.3 Volumetric Flow Rate Calculation 50
- 3.4 Uncertainty and Error Calculations 50
  - 3.4.1 Heat-Flux Uncertainty Calculation 51
  - 3.4.2 Volumetric Flow Rate Uncertainty Calculation 54
- 3.5 Heat Transfer Curves 62

Chapter 4 – Discussion and Conclusion 69

Chapter 5 – Recommendations 71

References 73

Bibliography 77

Appendices 78
Appendix A: Heat Flux and Temperature of Surface Calculation 79
Appendix B: Heat Flux and Temperature of the Heated Surface 80
Appendix C: Heat Transfer Coefficient Calculation 83
Appendix D: Heat Transfer Coefficient 84
Appendix E: Volumetric Flow Rate Calculation 87

List of Tables

Table 1: Volumetric Flow Rate on the Test Surface in (ml/min) for Different Pressures and Distance between the Test Surface and the Nozzle. 50

Table 2: Relation between Pressure and Total Volumetric Flux. 55

Table 3: Relation between Pressure and Spray Angle. 56

Table 4: Ratio between the Theoretical Coverage (W) and Distance (H) at Various Spray Angles. 56

Table 5: Relationship of the Pressure Head at the Nozzle to the Distance (H). 57

Table 6: Maximum and Minimum Ratios for a Spray Angle of 60°. 59

Table 7: Comparison between Present and Previous Works. 67

Table 8: Heat Flux and Temperature of the Heated Surface for H=3mm. 80

Table 9: Heat Flux and Temperature of the Heated Surface for H=7mm. 81

Table 10: Heat Flux and Temperature of the Heated Surface for H=12mm. 82

Table 11: Heat Transfer Coefficient for H=3mm. 84

Table 12: Heat Transfer Coefficient for H=7mm. 85

Table 13: Heat Transfer Coefficient for H=12mm. 86

List of Figures

Figure 1: Spray Volumetric Flux Distribution for Uniform Point Source. 3

Figure 2: Boiling Curves for Different Flow Rates at ΔT_{sub} = 27°C for (a) Nozzle 1, (b) Nozzle 2, and (c) Nozzle 3. 5

Figure 3: Surface Heat Flux and Expulsion Rate During Spray Cooling with Surfactant Solution (mass flux = 0.538 kg/m^{2}s). 7

Figure 4: Experimental Apparatus. 8

Figure 5: Copper Bar Side and Top Views. 9

Figure 6: Comparison of Mass Flow Rates for Smooth Surface. 10

Figure 7: Comparison of Temperature Rise as Function of Power for Varying Jets Sizes and Flowrates. The Case of No Jet (No Flow) is Given for Reference. 16

Figure 8: Typical Boiling Curve for Water at 1 atm: Surface Heat Flux q", as a Function of Excess Temperature, $\Delta T_e \equiv T_s - T_{sat}$. 23

Figure 9: Trends of the Heat Transfer Coefficient for a Horizontal Evaporator Tube. 25

Figure 10: Schematic View of the 1-D Inverse Heat Conduction Problem (IHCP). 27

Figure 11: Schematic of Experimental Apparatus. 33

Figure 12: Schematic View of the Fluid System. 34

Figure 13: Two-Stage Control Valves. 35

Figure 14: Schematic View of the Heater System. 37

Figure 15: Copper Cylinder (Cartridge Holder). 38

Figure 16: Variable Autotransformer. 39

Figure 17: SCXI System Components (National Instruments). 40

Figure 18: Installation of Thermocouples in the Terminal Block SCXI-1303). 41

Figure 19: Front Panel Designed for the Experiment. 42

Figure 20: Distance (H) Affecting the Sprayed Area. 44

Figure 21: Distance (H) Affecting the Volumetric Flow Rate. 44

Figure 22: Heat Transfer Coefficient Vs Heat Flux for Different Volumetric Flow Rate at H=3mm. 48

Figure 23: Heat Transfer Coefficient Vs Heat Flux for Different Volumetric Flow Rate at H=7mm. 49

Figure 24: Heat Transfer Coefficient Vs Heat Flux for Different Volumetric Flow Rate at H=12mm. 49

Figure 25: Uncertainty of the Spatial Separation between Thermocouples. 52

Figure 26: The Temperature Dependence of the Thermal Conductivity of Selected Solids. 53

Figure 27: Relation between Pressure and Total Volumetric Flux. 55

Figure 28: Spray Coverage. 57

Figure 29: Heat Transfer Curve for H=3mm and Different Volumetric Flow Rates. 63

Figure 30: Heat Transfer Curve for H=7mm and Different Volumetric Flow Rates. 64

Figure 31: Heat Transfer Curve for H=12mm and Different Volumetric Flow Rates. 64

Figure 32: Heat Transfer Curve for V=336.6ml/min and Different H. 65

Figure 33: Heat Transfer Curve for V = 464.6ml/min and Different H. 65

Figure 34: Heat Transfer Curve for P = 20 psi (V = 523.8 ml/min for H = 3 mm and 7 mm; V = 484.28 ml/min for H = 12 mm) at Different H. 66

Figure 35: Heat Transfer Curve for P = 25 psi (V = 583 ml/min for H = 3 mm and 7 mm; V = 440.83 ml/min for H = 12 mm) at Different H. 66

Figure 36: Heat Transfer Curve for P = 30 psi (V = 627 ml/min for H = 3 mm and 7 mm; V = 474.1 ml/min for H = 12 mm) at Different H. 67

Figure 37: Comparison between Present and Previous Works. 68

List of Symbols

Letters:

A	area	(mm^2, m^2)
C	constant	
d_{32}	Sauter mean diameter	(μm, mm)
d_n	jet diameter	(μm, mm)
f	frequency of the bubbles	(Hz)
h	heat transfer coefficient	($W/m^{2\circ}C$)
G	volumetric flux	($ml/s/mm^2$)
H	distance from test surface to nozzle	(mm)
k	thermal conductivity	($W/cm^{2\circ}C$, W/m^2K)
L	length of the test surface	(mm)
$\dot{m}$	mass flow rate	(kg/min)
P	pressure	(psi)
q	heat transfer	(W)
q”	heat flux	(W/cm^2, W/m^2)
Q	power input, heat lost	(W)
T	temperature	(°C)
U	uncertainty	
V”	volumetric flow rate impacting a surface	(ml/min)

$\bar{V}$”	mean volumetric flow rate	(ml/min)
W	theoretical coverage	(inch, mm)
x	position	(mm)
$\bar{x}$	sample mean	(mm)

Abbreviation:

CHF	critical heat flux	(W/cm^2, W/m^2)
CSC	cryogen spray cooling	
Cu	copper	
IP	input power	(W)
LDA	laser-doppler anemometry	
MEMS	micro-electro-mechanical system	
Na	activate nucleation site density	
Ni	Nickel	
Si	Silicon	
TIR	internal reflectance technique	

Greek Symbols:

Θ	sprayed angle	(°)
Δ	difference	
ƛ	thermal conductivity	($W/m^{2\circ}C$, $W/m^{2\circ}K$)
σ^2	variance	
σ	standard deviation	
Φ	diameter of the test surface	(mm)

Subscripts:

0	initial status
f	fluid
m	arithmetic means
max	maximum
sub	subcooling
sat	saturation
T	total
w	test surface, wall

Study of Upward-Facing Spray Cooling with Water at Atmospheric Pressure

Alberto D. Sato

ABSTRACT

Spray cooling is a high heat removal technique which has been used widely in many industries, especially metallurgical, where the control of the temperatures of metals is an important factor to obtain the desired microstructure; and also in microelectronics where is very important to obtain high heat fluxes at relatively low surface temperatures.

In this study, an open loop spray cooling system has been fabricated to provide an upward-facing spray over a 12 mm diameter test surface. A full cone spray nozzle was used to deliver deionized water to the test surface at five pressures (10, 15, 20, 25 and 30 psi), and at three different distances to the test surface (3, 7 and 12 mm). The volumetric flow rate at the surface used in the experiments depended on both the pressures and the distances. For a distance of 3 mm and 7 mm, the volumetric flow rate range from 336.6 to 627 ml/min while for 12 mm, the range was from 336.6 to 484.28 ml/min.

Heat fluxes of 1.92 to 451 W/cm^2, 2.1 to 417.3 W/cm^2 and 1.9 to 409.5 W/cm^2 for distances of 3, 7 and 12 mm respectively were registered at different

input power levels. For all the three distances, the volumetric flow rate affects the heat flux, especially for 3 mm; and this effect decreases for higher distances. However, the distance between the nozzle and the test surface has little effect on the heat flux at low pressures but at higher pressures, the difference in heat flux is mainly due to the fact that part of the spray does not impinge the test surface.

Chapter 1 – Background

Spray cooling is a very well known method used to dissipate high heat fluxes from heated surfaces. Sprays are produced by nozzles which drastically affect their characteristics: Sauter mean diameter (d_{32}), droplet velocity and volumetric flow rate. There are many types of nozzles but the most common is the pressure nozzle; and the most widely used pressure nozzle is the full cone spray-nozzle.

The experimental studies of spray cooling can be classified into two categories according to the way they are conducted [1].

a. Non-stationary methods: In this method the metal sample is heated to the desired temperature, then the heat is withdrawn and simultaneously the sample is wetted by the spray. Finally, the sample temperature decay versus time is recorded.
b. Stationary methods: In this method the metal sample is heated continuously by a controlled heating energy source in order to maintain its surface temperature constant during spraying the liquid.

The temperature of the metal sample greatly affects the heat transfer during the spray cooling stage. At relatively low temperatures, heat transfer is

caused mainly by steady-state boiling in which three distinct regions exist: forced convection and evaporation, nucleate boiling region, and critical heat flux. At higher temperatures, heat transfer is caused mainly by transient cooling in which film boiling and transition boiling exist [2].

Spray cooling is of great importance in various industries such as metallurgy, microelectronics, nuclear-power, etc; especially microelectronics where this method is used to remove high heat fluxes (>1000 W/cm^2) from surfaces with a considerably low wall superheat.

1.1 Literature Review

There has been little research done on upward-facing spray cooling; most investigations have been focused on downward-facing spray cooling. Rybicki, J. R., et al [3] compared single-phase and two-phase cooling characteristics for upward-facing and downward-facing sprays. In this experiment, PF - 5052 (dielectric coolant) was used as a working fluid which was sprayed over a square heated test surface made of copper (1.0 cm^2). Three full-cone spray nozzles were used to span a broad range of volumetric flow rates:

- Nozzle 1: $V'' = 35 \text{ to } 52\ m^3s^{-1}/m^2$
- Nozzle 2: $V'' = 83 \text{ to } 101\ m^3s^{-1}/m^2$
- Nozzle 3: $V'' = 113 \text{ to } 186\ m^3s^{-1}/m^2$

Boiling curves were generated by raising the voltage across the cartridge heaters in small increments and recording the heat flux from the test surface, the surface temperature, and the nozzle inlet temperature. The boiling data were

recorded after reaching steady-state. Steady-state was attained when the temperature variation was 0.1 °C or less during a 10 - minute period.

Rybicki studied the hydrodynamic characterization of a spray, especially two very important hydrodynamic parameters: volumetric flow rate, V", and d_{32}. The volumetric flow rate is non-uniform along the heated surface, as is shown in Figure 1.

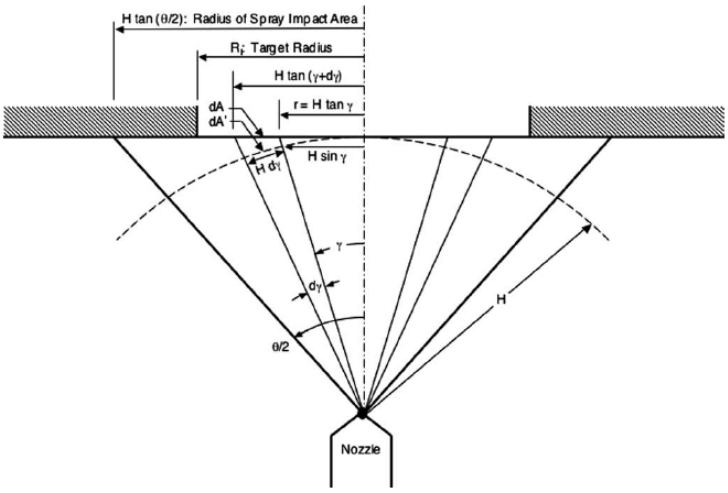

Figure 1: Spray Volumetric Flux Distribution for Uniform Point Source [3].

The investigator used the figure to develop the following equation, in which the mean volumetric flux is the total spray flow rate divided by the impact area.

$$\bar{V}'' = \frac{V''_T}{\pi \{H \tan (\theta/2)\}^2} \qquad (1)$$

This model is used to predict the flow rate distribution on the surface. At the center of the surface, the flow rate is maximum. This behavior affects the cooling uniformity and the Critical Heat Flux (CHF). The low flow in the outer regions means that the CHF will start sooner at the perimeters.

The distance between the nozzle and the test surface also has a strong influence on the CHF. Mudawar, I., and Estes, K. A. [4], demonstrates experimentally how large and small distances between the nozzle and surface yield relatively poor CHF. Large distances cause a large portion of the droplets to fall outside the test surface while small distances yield a small droplet impact area. The highest CHF was achieved when the impact area just inscribed the test surface:

$$H \tan(\theta/2) = L/2 \qquad (2)$$

L: Length of the test surface

The results obtained by Rybicki show that increasing flow rate generally enhances single-phase heat transfer and CHF, but the effect on the nucleate boiling region is very limited (as shown in Figure 2). The effect of subcooling is weak in the single-phase region but like flow rate, increasing subcooling yields an increase in CHF for each of the three nozzles. Similar results were observed when decreasing the droplet diameter which has been done utilizing different nozzles and pressures. This result obtained by Rybicki contradicts the results obtained by Chen, R. H., et al [5] who reported that d_{32} does not have a definite effect on the CHF.

Another important result of this experiment is that the single-phase heat transfer data for upward-oriented and downward-oriented sprays can be fitted using a correlation based on the Reynolds number of the spray and the Prandtl number of the liquid; and for nucleate boiling, they can be fitted using a correlation based on density ratio, Weber number and Jacob number. All these

correlations show that the spray orientation has virtually no effect on spray cooling performance.

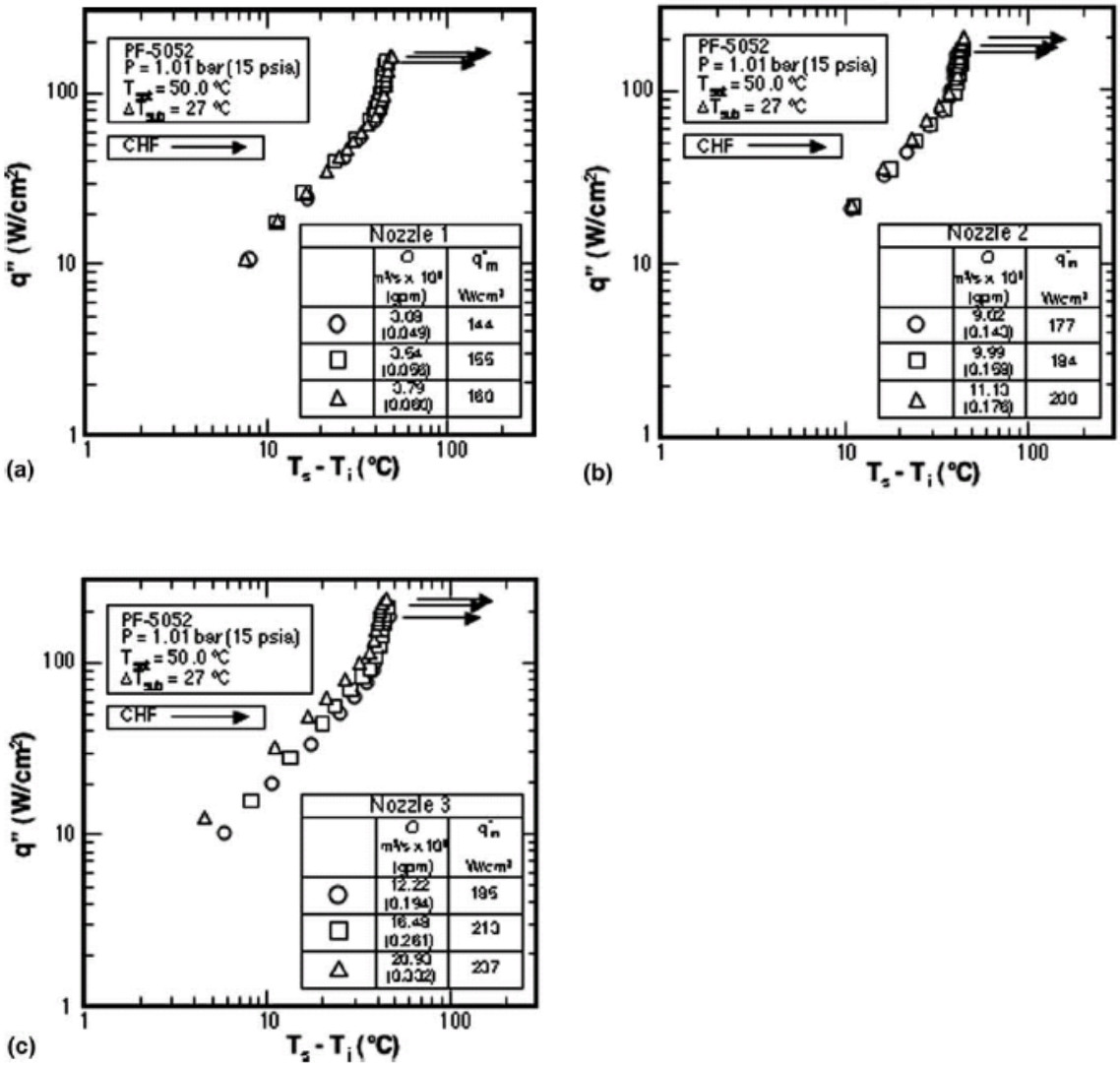

Figure 2: Boiling Curves for Different Flow Rates at ΔT_{sub} = 27°C for (a) Nozzle 1, (b) Nozzle 2, and (c) Nozzle 3 [3].

Many researchers studied a downward-facing spray over a heated surface. Jia, W., and Qiu, H. [6] studied the droplet dynamics and heat transfer for spray cooling of a 10 - mm diameter, horizontal copper surface using

deionized water and surfactant solution as working fluids. To produce the spray, a multi-nozzle (5) spray system was constructed in order to study the effect of mass flux on spray cooling. The mass flux spray varied from 0.156 to 1.20 kg/m^2. The characterization of the droplets was done by a laser-Doppler anemometry (LDA).

They identified four different regions in the boiling curve (as shown in Figure 3):

- Region I: In this region, the surface temperature is lower than 100 °C and the heat flux maintains a low value.
- Region II: In this region, the surface temperature reaches a few degrees higher than 100 °C and the heat flux increases rapidly (nucleate boiling).
- Region III: In this region, the heat flux increases but not as rapidly as in region II due to the heat transfer mechanism changes from the nucleate boiling to droplets evaporative cooling gradually.
- Region IV: In this region the film boiling starts.

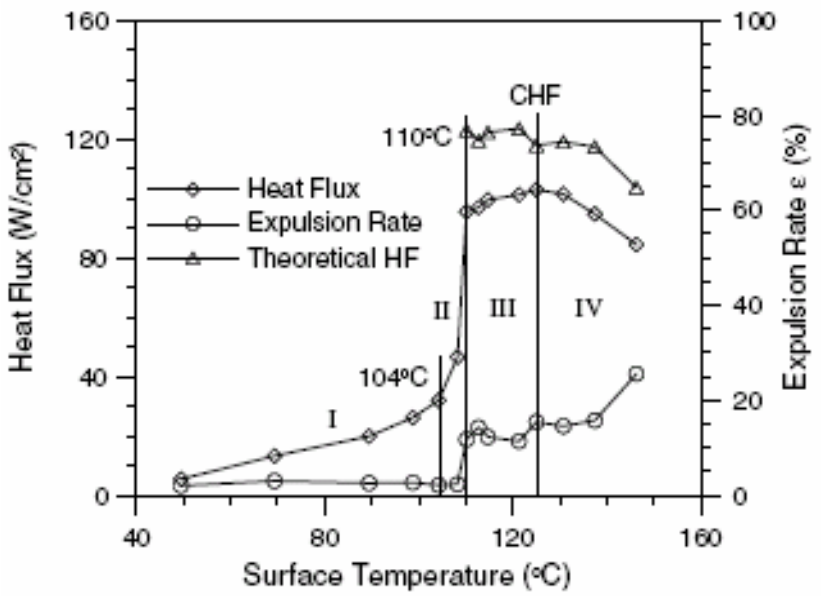

Figure 3: Surface Heat Flux and Expulsion Rate During Spray Cooling With Surfactant Solution (mass flux = 0.538 kg/m^{2}s) [6].

Results obtained in this experiment show that the critical heat flux (CHF) increases with the mass flux of water, and the surfactant addition in the solution shows a significantly advantage over pure water. In the boiling curve, the CHF temperature is moved to the left due to an increment of surfactant in the solution. This low CHF temperature means a high heat flux at relatively low temperatures which is very useful in multiple applications, especially microelectronics.

Lin, L., and Ponnappan, R. [7] studied the heat transfer characteristics of spray cooling in a closed loop using a 1 x 2 cm^2 test surface and FC - 87, FC - 72, methanol and water as working fluids. In this experiment, eight miniature nozzles in a multi-nozzle plate were used to generate a spray array. The results from this experiment corroborate that the volumetric flux of the working fluid drastically affects the heat flux due to the fact that higher volumetric flux implies a thicker liquid film that decreases the evaporation from the free surface and

increases the convection. Lin and Ponnappan found that Spray cooling can dissipate heat fluxes up to 90W/cm^2 with fluorocarbon fluids, 490 W/cm^2 with methanol and heat fluxes over 500 W/cm^2 with water.

Ortiz, L., and González, J. E. [8] investigated steady-state high heat fluxes using spray cooling on a 1.25 cm diameter test surface using distilled water as a working fluid. The experimental apparatus consisted on three major systems: the heater, the fluid delivery, and the data acquisition systems (as shown in Figure 4). The heated surface consisted of a copper bar with 3.5 cm base and 16.64 cm length, but the diameter of the test surface was reduced to 1.25 cm diameter because this reduction increases the heat flux at the tip of the copper bar. The copper bar was drilled three times from the test surface at different distances and separated by 120° at each level; in those holes, nine K-type thermocouples were inserted (as shown in Figure 5).

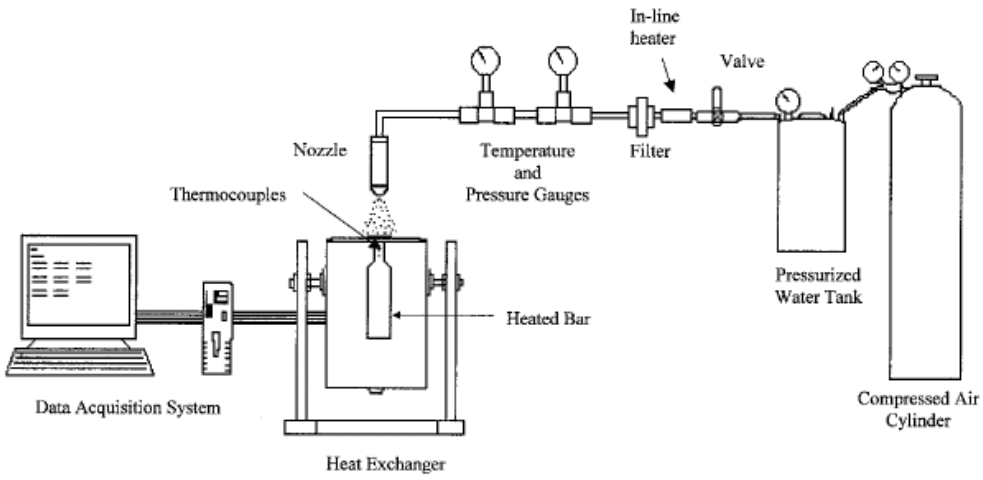

Figure 4: Experimental Apparatus [8].

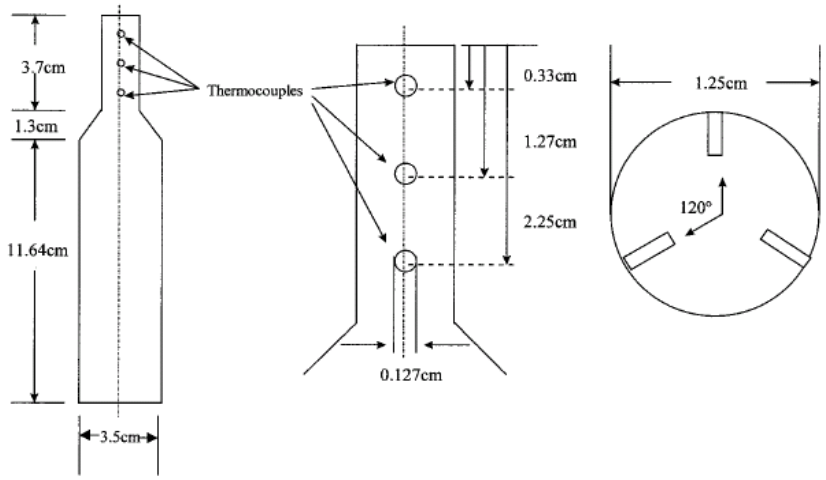

Figure 5: Copper Bar Side and Top Views [8].

The nozzles utilized were full cone WDB - 0.5 with 0.0211 cm orifice diameter at 45° cone angle, and WDB - 1.0 with 0.0279 cm orifice diameter at 30° cone angle for which flow rates ranged between 1.48 and 2.91 l/h.

Ortiz calculated the heat flux, using the temperature gradient provided by the three levels of thermocouples and Fourier's Law:

$$q'' = k \frac{\Delta T}{\Delta x} \qquad (3)$$

Where k is the thermal conductivity of copper, ΔT is the difference between the temperatures of two thermocouple levels, and Δx is the distance between these thermocouples levels.

The sets of experiments were done at steady-state which means that the copper bar was heated slowly while the heated surface was sprayed until the surface temperature remained constant for more than 15 minutes.

The results from this experiment clearly confirm that high flow rates produce high heat fluxes (as shown in Figure 6). They also studied the effects of surface roughness, subcooling and impact angle on the heat flux. Smooth

surfaces produced lower steady-state high heat fluxes than rough surfaces due to the fact that rough surfaces have more nucleation sites to produce bubbles. Increment in subcooling temperature decreases the heat-flux removal capacity for smooth surfaces, but increases the heat-flux for rough surfaces. Finally, increments in the impact angle decrease the heat removal capacity because inclination induces sprayed water to fall, decreasing the opportunity to maintain a liquid thin film over the surface.

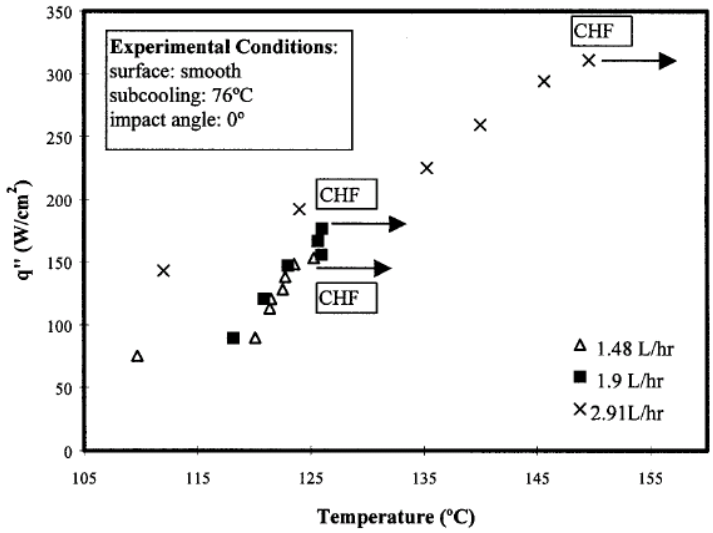

Figure 6: Comparison of Mass Flow Rates for Smooth Surface [8].

Horacek, B., et al [9], studied the heat transfer mechanisms for single nozzle spray cooling, using different amounts of dissolved gas. In this experiment, a full cone spray nozzle was used to cool a microheater array that consisted of 96 heaters and total area of 0.49 cm^2 (7.0 mm x 7.0 mm). The spray nozzle was oriented normal to the microheater array and located 17 mm from the surface. The flow rate was set at 32 ml/min and FC - 72 was used as the working fluid. The results clearly suggest that thermal subcooling increases the heat

transfer for a given flow rate which confirm the results of previous researchers. Dissolved gas shifts spray cooling curves to the right and CHF increases with increasing gas content due to the fact that dissolved gas increases the T_{sat} (temperature of saturation) of the fluid. Visualization and measurements of the liquid-solid contact area and the three-phase contact line length were made by using a total internal reflectance technique (TIR). At low wall superheats, the surface was almost completely wet by liquid but at higher wall superheats (near CHF) the surface was mainly covered by intermediate-sized droplets. Beyond CHF (film boiling), part of the heater appeared completely dry out.

Jiang, S., and Dhir, V. K. [10] studied the effect of the presence of non-condensibles in a closed system on the heat transfer coefficient in single phase and boiling modes. The test surface was 20 mm in diameter made of copper which was sprayed with deionized water. The distance between the nozzle and the test surface was constant at 13 mm. In this experiment, the system total pressure was set at 56 kPa, 72.5 kPa and 101 kPa while varying the vapor pressure inside the chamber from 2.32 kPa to 97.9 kPa. The results from this experiment show that the heat flux increases from the single phase regime to partial nucleate boiling regime; this increment is more discernible for vapor pressure of 2.32 kPa. This experiment also shows a little increment of heat flux when the temperature of subcooling increases. The system total pressure has little effect on the heat transfer coefficient in single phase regime but after boiling, higher total pressures yield higher heat flux for the same wall superheat.

Fabbri, M., and Dhir, V. K. [11] studied the heat transfer under arrays of microjets using deionized water and FC40 as test fluids. The test surface was a 19.3 mm diameter copper cylinder, which represented the backside of an electronic microchip. Results from this experiment show that arrays of microjets produces the same heat flux rate as a few large jets but with lower coolant flowrates. Another interesting result is that there is only a small affect of the distance between the microjets and the test surface, however at very large distances, the jets may become hydrodynamically unstable and break up into droplets.

Many researchers studied cooling of heated surfaces by jet or micro-jet cooling devices which were created with specific parameters like: internal angle, shape of the orifice, inner-diameter of the orifice, etc. Wang, E. N., et al [12] studied two-phase microjet impingement cooling in a confined geometry test device. In this experiment, circular jets with diameters less than 100 μm were machined in glass and heater/sensor test structures were fabricated to examine heat transfer and microjet characteristics. Two separate heater devices were fabricated, one for uniform heating and the other for simulating the presence of a chip hotspot. The results show heat transfer coefficients of approximately 1000 $W/m^2°C$ at the stagnation point and 700 $W/m^2°C$ at 1.5 mm away from the stagnation point were achieved. Again, in this experiment the flow rate had a great affect on the heat flux. Increasing the flow rate from 0.75 ml/min to 1 ml/min for the same size jet, the temperature at the stagnation point was decreased by 15% (from 80 °C to 70 °C).

Another investigation into jet cooling by an array was done by Oh, C. H. et al [13] who studied high heat flux removal by liquid-jet array cooling modules. The orientation of the spray was upward-facing, impinging on a faceplate (10 cm^2) heated by a thin film heater. Heat fluxes of up to 17 MW/m^2 were produced and temperature differences of up to 500 °C between the heater surface and the average bulk temperature of the water were measured. The graphs of temperature difference Vs heat flux show a linear relationship between both parameters, which suggest that cooling was entirely convective without boiling. In this experiment, the modules could dissipate fluxes above 20 MW/m^2 but difficulties with the heating element prevented the study of such high fluxes.

Spray cooling and liquid jet impingement cooling were compared and studied by Oliphant, K. et al [14] in the non-boiling region. The experimental apparatus consisted of a heated surface made of aluminum with a1.9 cm diameter. The delivery fluid system consisted of two different jet arrays, one with 7 holes and the other with 4 holes, using two different jet diameters: 1.0 and 1.59 mm, and a commercially available spray nozzle with Sauter mean diameter of 50 μm and velocity of approximately 3.0 m/s. Results suggest that the heat transfer depends on the number and velocity of the impinging jets; and contrary to the results of other researchers, Oliphant suggests that spray cooling does not have a definitive dependence on mass flux. Spray cooling and jet impingement can be used to provide the same heat transfer rates, but spray uses significantly lower mass flux.

Many researchers focused their studies on the behavior of the droplet(s) impacting a heated surface. Kizito, J. P., et al. [15], is one of many researchers who studied, theoretically and experimentally, the behavior of a single droplet impacting a heated substrate. Kizito investigated experimentally the behavior of a droplet impacting a heated surface using a high-speed camera (2000 frames/sec). In this experiment, the temperature of a heated billet was held constant during the droplet impact. The droplet velocities were increased or decreased by translating the release mechanism vertically, using gravitational force. They also used many types of fluids which included alkanes, alcohols and deionized water. Results from this experiment suggests that the heat transfer from the surface to the droplet is maximum in the case where the droplet has the widest extent of spread on the substrate and does not splash.

Other researchers who investigated the behavior of droplets impacting a heated surface are Kandlikar, S., and Steinke, M. E. [16]. They studied the contact angles of droplets during spread and recoil after impinging on a heated surface. The experimental setup consisted of a heated surface which was impinged by a water droplet from a droplet delivery system and the droplet dynamics were captured by a high-speed digital camera. Many materials were used as a heated surface and each one with different surface roughness values; the SilverStone surface had a surface roughness of 1.35 μm; the copper surface was prepared with surface roughness of 0.63 μm, 0.32 μm, 0.25 μm, and 0.02 μm; the stainless steel surface had a surface roughness of 0.13 μm, 0.07 μm, 0.04 μm, and 0.01 μm. The results show that the behavior of the contact angle

was different depending on the material of the heated surface. For copper, the contact angle increases for the smoothest surface while is the opposite for stainless steel. Another result is that the temperature of the heated surface affects the behavior of the impinged droplet and its contact angle. The contact angle is very important in spray cooling to predict the maximum spreading ratio of the droplet, which will affect the heat transfer.

Studies of the behavior of impinging droplets on a very high temperature plate was investigated by relatively few researchers due to the difficulty of achieving high test surface temperatures. Hatta, N. et al [17] investigated the collision dynamics of a water droplet impinging on a heated surface above the Leidenfrost point. In this experiment droplets from 300 to 700 μm in diameter were generated with an impinging velocity range between 1.2 and 6.0 m/s. These droplets impinged a 28 mm diameter Inconel alloy 625 test surface which was held at 500 °C throughout all the experiments. The deformation process of the droplet was recorded using a video camera; from which the critical Weber number between rebounding and disintegration effects could be calculated. Their calculated critical Weber number of nearly 50 was relatively small compared with other researchers as Ueda et al [18], who obtained a critical Weber number of 70 using droplets between 2 to 3 mm and stainless steel and copper surfaces heated at 300 °C. Another important conclusion obtained in this experiment is that the rebounding condition is influenced not only by the critical Weber number but by surface temperature, surface roughness, surface material, and many other parameters.

Investigations of cooling techniques in microelectronics have been investigated in the past 6 years; some of them investigated a spray array configuration to cool down VLSI chips. Wang, E. N. et al [19]; studied the effect of the diameter of micro-jets and the volumetric flow rate on the temperature profile of a heater/sensor test structure. Their results show that the difference in jet diameter (d_n) had little effect on the temperature profile for this range of parameters (d_n = 50 μm, and 70 μm jet, and V" = 0.75 ml/min); but the flow rates had a great affect on the temperature profile (shown in Figure 7).

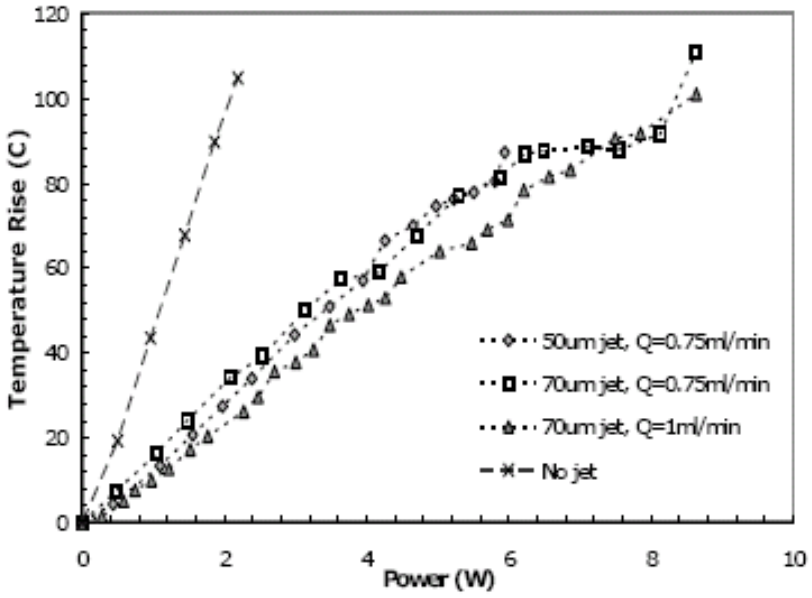

Figure 7: Comparison of Temperature Rise as Function of Power for Varying Jets Sizes and Flowrates. The Case of No Jet (No Flow) is Given for Reference [19].

Bash, C. E. et al [20], studied a new method to address non-uniform high-power density in electronic applications. The new method consisted of a thermal inkjet assisted spray cooling which included a Hewlett-Packard cartridge with two rows of 256 nozzles. Each nozzle could be controlled independently from the others using a control mainframe. The heated surface was a 22.5 mm x 12.5 mm

copper block, with K-thermocouples embedded in it, in order to measure the surface temperature. Results show that heat fluxes up to 270 W/cm^2 can be dissipated with water while maintaining a high coefficient of performance.

Another investigation of great importance for computers was done by Garimella, S. V. [21], who studied an impingement-cooled system. He studied the effects of working fluids, pressure drop, type of heated surface and type of cooling fluid configuration (suction Vs impingement configuration). Pressure drop is a very big problem in impingement-cooling due to higher-pressure drop means higher input power in the system. Brignoni suggests that a simple modification of the orifice inlet shape, can reduce the pressure drop by 31% without affecting the cooling rates [22]. Another improvement of the cooling system could be done by employing extended surfaces and heat sinks mounted on the heat source. Brignoni and Garimella [23] show a relatively high increment of the cooling rates for the heat sink relative to the bare surface by a factor of 2.8 to 9.7. Finally, Garimella presents the benefits of each cooling fluid configuration; in the case of suction arrangement, there is the greatest surface-to-coolant temperature difference at lowest-velocity air. In the case of impingement configuration, there is a higher effectiveness of heat removal than for the suction configuration [24].

Micro-jets were studied for microelectronics by many researchers. Wu, S. et al [25], investigated heat transfer using micro-electro-mechanical system (MEMS) impinging jets. A MEMS sensor chip was designed and fabricated with an 8 x 8 temperature array on one side. This sensor chip can measure a 2-D surface temperature with various jets impinging on it. A single glass nozzle, a

MEMs single nozzle, a MEMS nozzle array and a MEMS slot arrays were also fabricated for this experiment. Results from this experiment show that the cooling capability of a single glass jet increases with its driving pressure, and the MEMS single nozzle has similar cooling characteristics to a free jet at high distances between the nozzle and the microchip. But the results also show that lower pressures yield higher cooling efficiency for both single free jet and MEMS jet. This is very important because the design of an impinging jet cooling depends on the gas sources. In the case of jet array cooling, the temperature distribution is more uniform than single jet cooling, which increases its cooling efficiency.

Many researchers studied pulsed sprays which have important applications in many areas, especially in medicine where cryogen spray cooling is used to reduce the temperature of the skin when a laser is focused on it. Loureiro, H. M. et al [26] measured the droplet characteristics and thermal behavior in order to study pulsed spray cooling over a heated aluminum-plate. In this experiment, the spray was generated by a pintle - type injector and the frequency and duration of the injection were controlled by an arbitrary function generator. The working fluid was gasoline with a temperature of 31 °C. The results show that the transient behavior of the spray can be divided into three periods. The first period is characterized by a sudden expansion of the liquid, called *leading front of the spray;* the second period is characterized by an increase of the mean droplet axial velocity up to a steady - value, called *the steady spray*; the third and final period is characterized by an asymptotic decrease of the mean axial velocity down to 0 m/s. Another important result is

that the overall heat transfer coefficient increases when decreasing the pressure of injection and/or the duration of injection increases. Finally, at very high test surface temperatures, the behavior of the spray is affected because it enhances evaporation and induces secondary break-up of droplets. These very small droplets remain suspended in the air which affect the subsequent droplets.

Another important parameter studied in cryogen spray cooling was the variation of the initial temperature of the skin-surface. Jia, W. et al [27], investigated the heat transfer dynamics during cryogen spray cooling of substrates at different initial temperature. The experimental apparatus consisted of a test surface made of aluminum with 10 mm x 10 mm area, and a cryogen delivery system with 0.7 mm - inner diameter and 63.6 mm - length nozzle, with tetrafluoroethane (R - 134a) as a working fluid. Results suggest that the maximum heat flux (q''_{max}) increases with increasing T_0 and decreasing the distance nozzle - surface (H); but the heat transfer coefficient (h) is not affected by T_0.

Other parameters that affect cryogen spray cooling (CSC) and were studied carefully by researchers are the droplet size and the spray density. Pikkula, B. M. et al [28] used four types of delivery devices: a fuel injector with 1.3 mm diameter, a second fuel injector with 1 mm diameter, commercial atomizers with 1 and 1.5 mm diameters, and a cryogen delivery device with 0.75 mm diameter; used to deliver cryogen R - 134 a. Results show that heat removal varied with the types of delivery devices, but those variations were less than 14%. This low variation was something strange due to the fact that relatively

large differences in mass output (greater than a factor of 6) and droplet sizes (greater than a factor of 2) among the devices were observed.

Continuing with parameters that affect CSC, Pikkula, B. M. et al [29], studied also the effect of droplet velocity, diameter, and film height on heat removal. The experimental methods included tetrafluoroethane (R-134a) as a working fluid, with a spurt duration set to 200 ms; and a substrate which was composed of epoxy resin with embedded micro-thermocouples to record internal temperature profiles. Results suggest that Weber number is sensitive to the variations in droplet velocity, and the heat removal is influenced by the Weber number (higher heat removal resulted from higher Weber number and higher velocity); also the cryogen film acts as an impediment to heat transfer between the impinging droplets and the substrate.

In spray cooling is important the angle of incidence of the droplets towards the heated surface. Many researchers investigated this parameter such as Aguilar, G. et al [30], who studied the influence of angle between the nozzle and skin surface during CSC. The distance between the nozzle and the test surface was maintained constant at 30 mm but the impinging angle was varied from 90° (perpendicular) to 15° in decrements of 15° plus an exaggerated angle of 5°. The working fluid was R - 134a which was delivered in three intervals with 50 ms duration. Results suggests that there is a minimal difference between the temperature behavior of the surface, heat flux and overall heat extraction, for the cases where the angle of incidence is between 90° to 15° but there is a relatively high difference (10% - 15%) for the 5° angle.

Volumetric flow rate is probably the parameter that highly affects the heat transfer performance. Kim, J. H. et al [31]; studied the effect of the volumetric flow rate on the heat transfer on plain and microporous surfaces of a flat heater. Their results suggest that for low heat flux (less than 10 kW/m^2), the flow rates (1.25, 1.75, and 2.4 ml/min) had no effect on the spray cooling curves; but for the case of higher heat fluxes, the heat transfer increased when the volumetric flow rate increased. These results seem contrary to the results suggested by Jiang, S. & Dhir, V. K. due primarily by the fact that spray cooling is very complex and its heat transfer behavior depends on so many parameters and on the range we are working these parameters.

The majority of the spray cooling experiments have been done using a relatively small test surface, but some researchers investigated experimentally the cooling of a large heated surface. Xishi, W. et al. [32], studied the effect of initial surface temperature and mist characteristics (droplet size, velocity, etc.) on a large heated surface. The experimental apparatus consisted of a pressure nozzle positioned 1000 mm above the surface which injected water mist to the hot surface; and a heated plate with 150 mm x 150 mm area, positioned 200mm away from the axis of the nozzle. The working pressures utilized for the nozzle were 0.2, 0.4, and 0.6 Mpa; and initial surface temperatures of 80, 100, and 120 °C were utilized for the test surface. Results show that the mist droplet cooling efficiency is affected by not only the initial surface temperature but by the mist characteristics, especially the Weber number. For all initial surface temperature,

the highest droplet cooling efficiency was obtained for a working pressure of 0.4 Mpa.

The parameters related to the fluid system in a spray cooling device, were studied by Estes, K. A., and Mudawar, I. [33]. They investigated the affects of three spray nozzles, volumetric flux, subcooling and working fluid on nucleate boiling heat transfer and CHF. The spray nozzles had different orifice diameter (from 762 to 1700 x 10^{-6} m), spray angle (from 55.8 to 48.5 degrees), volumetric flux (from 16.6 to 216 x 10^{-3} m^3s^{-1} m^{-2}), and d_{32} (from 110-214 x 10^{-6} m). The results show different boiling curve shapes for the three spray nozzles. Spray nozzles with low volumetric flux display a more pronounced increase in the slope of the boiling curve because of higher evaporation efficiency, while high volumetric flux display little increase in the slope because of a suppression of nucleation and reduced evaporation efficiency. The CHF increases with the flow rate and subcooling but decreases with larger diameter of the droplets. In general, CHF is influenced by thermophysical properties of the fluid (density, enthalpy, specific heat at constant pressure, etc.), flow parameters (subcooling, pressure drop, volumetric flux), orifice parameters (nozzle orifice diameter, spray cone angle), and heater length.

1.2 Heat Transfer Regimes

A typical boiling curve consists on four regimes: free convection, nucleate, transition and film boiling. Those regions have their own characteristics that make them unique with respect to the others.

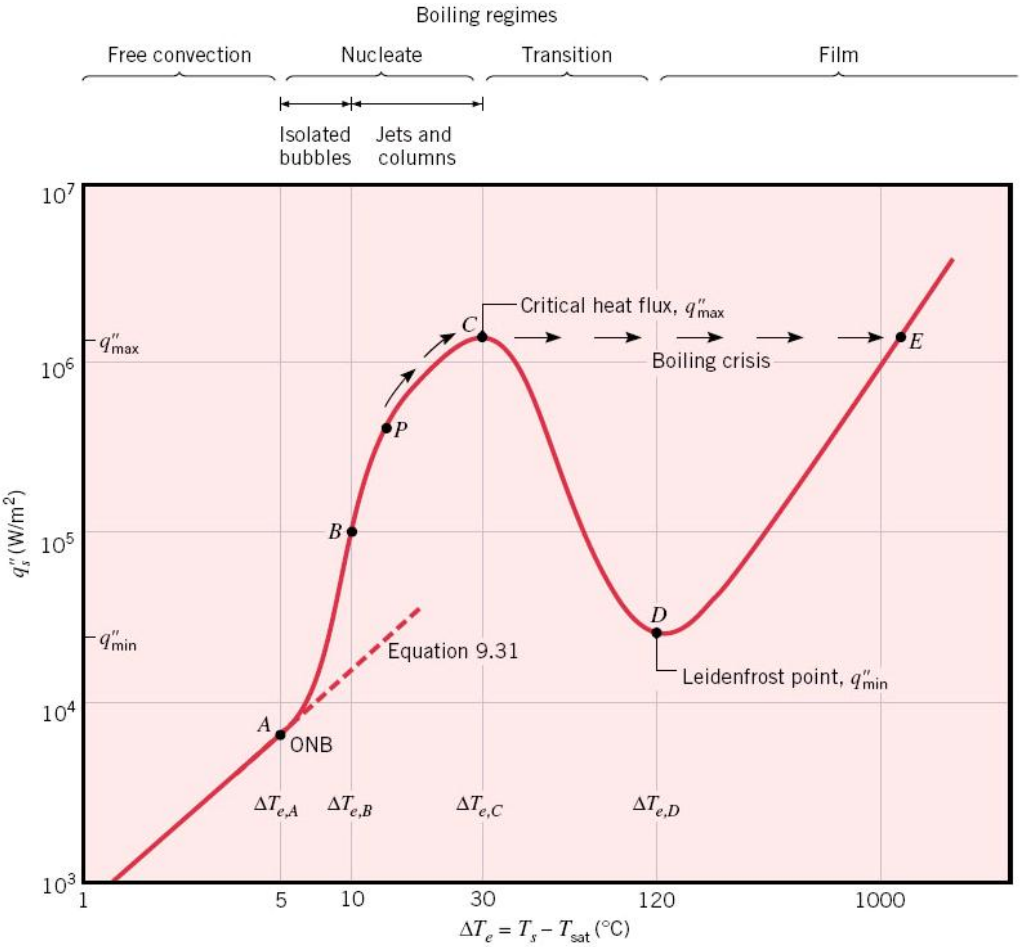

Figure 8: Typical Boiling Curve for Water at 1 atm: Surface Heat Flux q", as a Function of Excess Temperature, $\Delta T_e \equiv T_s - T_{sat}$.[34].

During the first regime (the straight line in Figure 8) the heat transfer is by natural convection, and there is no formation of vapor bubbles. During the second regime, between points (A) and (C), the growth of vapor bubbles at nucleation sites on the heated surface is observed. In this regime the frequency of bubble departure increases with surface temperature. The formation of these

bubbles increases the disturbance of the hot layer which raises the heat flux during this regime. The third regime begins after the CHF (point C in Figure 8) which is the critical or burnout heat flux that represents the end of nucleation boiling regime. In this region, also known as *Transition*, the increase in vapor production of the bubbles is so severe that the flow of liquid to the surface is restricted, producing a decrease of the heat flux. This reduction of heat flux continues until it reaches a minimum heat flux commonly known as the Leidenfrost point (point D in Figure 8). After this point, there is an increment of heat flux even greater than the CHF at much higher temperatures but because the surface is covered by a vapor layer, the heat transfer is due by radiation instead of thermal conduction (*Film Boiling*).

Baehr H. D. & Stephan, K. [35] described three types of boiling: evaporation, nucleate boiling and convective boiling; each one of them having different characteristics and behavior. Evaporation appears when the wall is heated to a temperature just above the saturation temperature, and there is only a few or even no formation of vapor bubbles. Nucleate boiling appears when the temperature of the wall is increased and vapor bubbles begin to form. Finally, in convective boiling, the local heat transfer coefficient is independent of the heat flux (q") but is strongly dependent on the mass flow rate and the quality of the vapor (see figure 9).

In order to understand nucleate boiling, it is very important to understand the bubble growth dynamics as Hewitt, G. F., et al [36] explains for the case of both spherical and isolated bubbles. In a first instance, the growth is dominated

by hydraulic and surface tension forces and the radius of the bubbles increases rapidly. After that, the bubble growth takes place because of a temperature gradient that exists between the superheated liquid/solid surface and the interface which means that the growth rate is governed by conduction heat transfer. Many other phenomenons affect the growth rate; for example, Shah, V. L., and Sha, W. T. [37], showed that the decrement of the thermal boundary layer thickness, due to the motion of the bubble, increases the growth rate. Van Stralen, S. J. D. [38] results suggest that the bubble growth rate is affected by the

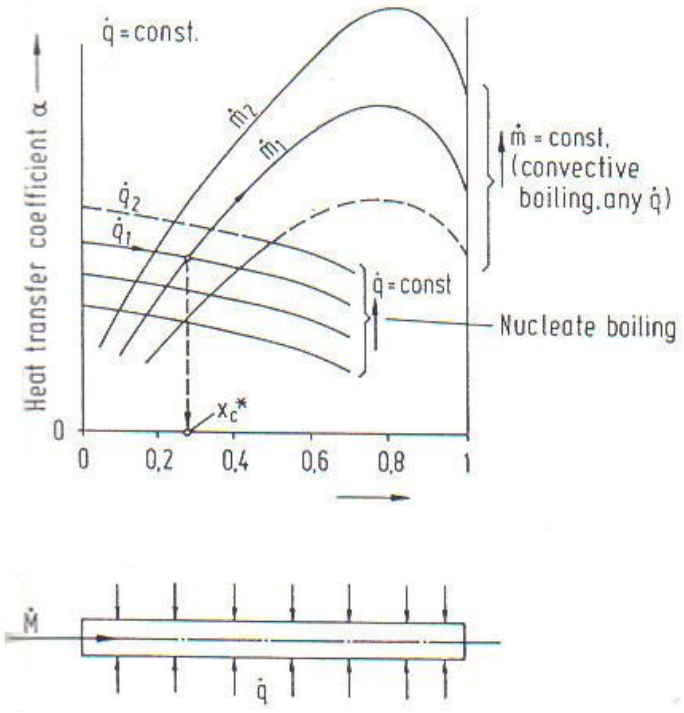

Figure 9: Trends of the Heat Transfer Coefficient for a Horizontal Evaporator Tube [35].

influence of neighboring bubbles. One big bubble can affect negatively the growth rate of another smaller neighbor because large bubbles absorb almost all the energy from the superheated liquid allowing little to be absorbed by the smaller ones.

1.3 Objectives of the Present Study

As stated in the literature review, there are many parameters that affect the heat transfer during spray cooling. One of these parameters is the direction of the spray (downward-facing, upward-facing or lateral spraying), which generally has been studied as downward-facing or even lateral spraying. There is almost no information about upward-facing spray cooling. In order to investigate this orientation and other parameters, these objectives are proposed:

1. To design an upward-facing spray cooling apparatus which will allow us to investigate some heat transfer performance.
2. To carry out experiments with the apparatus designed specially for this study in order to investigate how some parameters affect the heat transfer characteristics.
3. To explain the differences or similarities between the upward-facing and downward-facing spray cooling from this experiment and studies from other researchers.

1.4 Determination of Heat Flux and Surface Temperature

In this investigation as well as in other applications, the measurement of the surface-test temperature can not be done directly either because the installation of the thermocouple may disturb the experiment or because the environment is chemically destructive and could damage it. An inverse method was used to calculate the surface temperature and the heat flux in the copper cylinder. These estimations which involve internal measurements are associated

with errors and uncertainties that will affect the accuracy of the calculation of both surface temperature and heat flux.

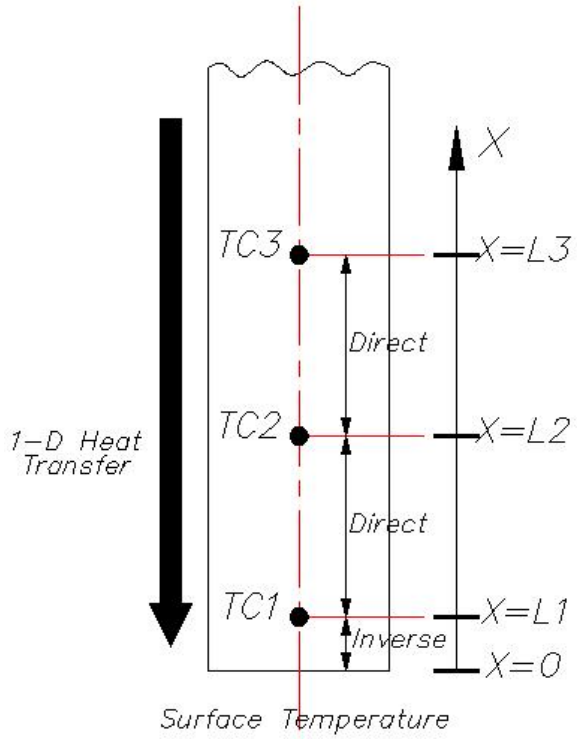

Figure 10: Schematic View of the 1-D Inverse Heat Conduction Problem (IHCP).

The heat flux between points “2” and “3” can be calculated using Fourier’s Law of conduction in 1-D.

For the present study, the surface heat flux was considered as a function only of a 1-D conduction problem, and the variation of the heat flux between points (2) – (3), and (1) – (2) were considered in order to calculate the heat flux between the surface and point (1). The heat flux between those points varied because of different causes, some of them were: the heat lost between those points was not equal (heat lost in the surface of the cartridge holder), or simply the contact between some thermocouples and the cartridge holder were better

than the others (the thermocouples were covered with a high thermal conductivity paste and then embedded into the cartridge holder).

There were two possible cases, one case when the heat flux along points (1)-(2) was greater than points (2)-(3) and the other case, the opposite. For the first case, which was the most common case, the heat flux in the surface was greater than the other two, and was calculated as follows:

A. Case $q''_{1-2} > q''_{2-3}$

The difference of the heat flux between points (1)-(2) and (2)-(3), ($q''_{1-2} - q''_{2-3}$), occurred along the points (1)-(3) or (L_3-L_1); but the difference between the heat flux between the surface and point(1), and (1)-(2), ($q''_{w-1} - q''_{1-2}$), occurred along the distance between the surface and point (2) or L_2 (see figure 10). This theory can be expressed as:

$$\frac{q''_{1-2} - q''_{2-3}}{q''_{w-1} - q''_{1-2}} = \frac{(L_3-L_1)}{L_2}$$

Then q''_{w-1} can be expressed as:

$$q''_{w-1} = q''_{1-2} + \frac{L_2 \, x \, (q''_{1-2} - q''_{2-3})}{(L_3 - L_1)} \qquad (4)$$

The temperature of the surface can be calculated using the previous heat flux:

$$T_w = TC_1 - \frac{L_1 \, x \, q''_{w-1}}{K_{Cu}} \qquad (5)$$

B. Case q"1-2 < q"2-3

This case is almost the same as the previous case, but the heat flux between the surface and point (1) was lower than the other two.

$$q''_{w-1} = q''_{1-2} - \frac{L_2 \, x \, (q''_{1-2} - q''_{2-3})}{(L_3 - L_1)} \qquad (6)$$

The temperature of the surface can be calculated using the same equation for the previous case.

1.5 Determination of Heat Transfer Coefficient

The heat transfer coefficient is considered a factor to calculate the heat transfer, and it is also considered as a thermal resistance due to the fact that it adds inversely like resistances [39].

$$q = h \, x \, A \, x \, (T_w - T_f) \qquad (7)$$

In this equation, h is used to calculate the input power or heat lost (q). The total heat removed, is dependent on the heat transfer coefficient and the area over which the spray systems acts. As an example of this, we can obtain the same amount of heat removed in a small surface impinged by a high pressure fluid and in a large surface impinged by a softer spray. Then the heat removal depends on how quickly the material can conduct the heat to the surface, and h can give us this important information.

There are two ways to determine the heat transfer coefficient, one of them is by steady-state experiments, and the other is by transient experiments. In this study, h was calculated using the following equation:

$$h = \frac{q''}{(T_w - T_f)} \qquad (8)$$

Where the heat flux (q") and the temperature of the test surface (T_w) were calculated using the temperature gradient obtained from the thermocouples

embedded in the cartridge holder (see subchapter 2.1). In this study, q" is divided by ($T_w - T_f$) instead of (T_w – Tsat) because the experiments were done in the single-phase regime instead of the boiling regime.

1.6 Uncertainty and Error Analysis

An error is always inherent in a measurement; that means even using the most accurate instrument, there still are errors. Barry, B. A.[40] describes two different types of errors: systematic errors (also called cumulative errors) and accidental errors (random errors, usually not cumulative errors). Systematic errors are subdivided in: natural errors (like refraction of light rays, thermal expansion of materials, etc.), instrumental errors (like bad calibration of the instrument) and personal errors (by physical limitations or bad habits of the observer).

In order to study errors, is very important to perform statistical analysis. Statistics can be used to determine the dispersion (or uncertainty) of the data, from which variation and standard deviation are probably the most common methods. Beauford, J. [41] in the book: *"Statistics in Science"* describes important statistics tools like: mean median, mode, variance and standard deviation.

- Sample mean: $\bar{x} = \frac{\Sigma x}{n}$ (9)

- Variance (entire population): $\sigma^2 = \frac{\Sigma (x-\bar{x})^2}{n}$ (10)

- Standard Deviation (entire population): $\sigma = \sqrt{\sigma^2}$ (11)

It is important to know the difference between error and uncertainty. An error is used for the cases of bad measurement by the observer and by bad measurement scale, but an uncertainty is used for inaccuracy of measurement results. In order to estimate the uncertainty for a result involving measurements of several independent quantities, it is necessary to know the following theory:

A. If the desired result is the sum or difference of two measurements, then the absolute uncertainties add.

$$Z = x + Ux + y + Uy = x + y + Ux + Uy \quad (12)$$

For independent errors with normal distribution or Gaussian Distribution, the uncertainty for the result can be expressed as:

$$Uz = \sqrt{Ux^2 + Uy^2} \quad (13)$$

B. If the desired result involves multiplying (or dividing) measured quantities, then the relative uncertainty of the result is the sum of the relative errors in each of the measured quantities.

$$Z = \frac{x_1 x_2 x_3 \ldots}{y_1 y_2 y_3 \ldots}$$

$$\ln z = \ln x_1 + \ln x_2 + \ln x_3 + \ldots - \ln y_1 - \ln y_2 - \ln y_3 - \ldots$$

$$\delta(\ln z) = \frac{dz}{z} = \frac{dx_1}{x_1} + \frac{dx_2}{x_2} + \ldots - \frac{dy_1}{y_1} + \frac{dy_2}{y_2} + \frac{dy_3}{y_3} - \ldots$$

Simplifying: $$\frac{Uz}{z} = \Sigma_i \left(\frac{Ux_i}{x_i} \right) + \Sigma_i \left(\frac{Uy_i}{y_i} \right) \quad (14)$$

For independent errors with normal distribution or Gaussian Distribution, the uncertainty for the result can be expressed as:

$$\frac{U_z}{z} = \sqrt{\left[\sum_i \left(\frac{U_{x_i}}{x_i} \right)^2 + \sum_i \left(\frac{U_{y_i}}{y_i} \right)^2 \right]} \qquad (15)$$

Chapter 2 - Experimental Methods and Procedures

Presented in this chapter are descriptions of the experimental apparatus and the methods and procedures used to perform the experiments. The experimental apparatus shown in Figure 11 consisted basically of three systems: fluid system, heater system, and acquisition system. Each system consisted of many devices which allow for the measurement of heat fluxes along a heated copper cylinder sprayed by deionized water. The methods and procedures are described in detail in order to demonstrate the credibility of the experiment.

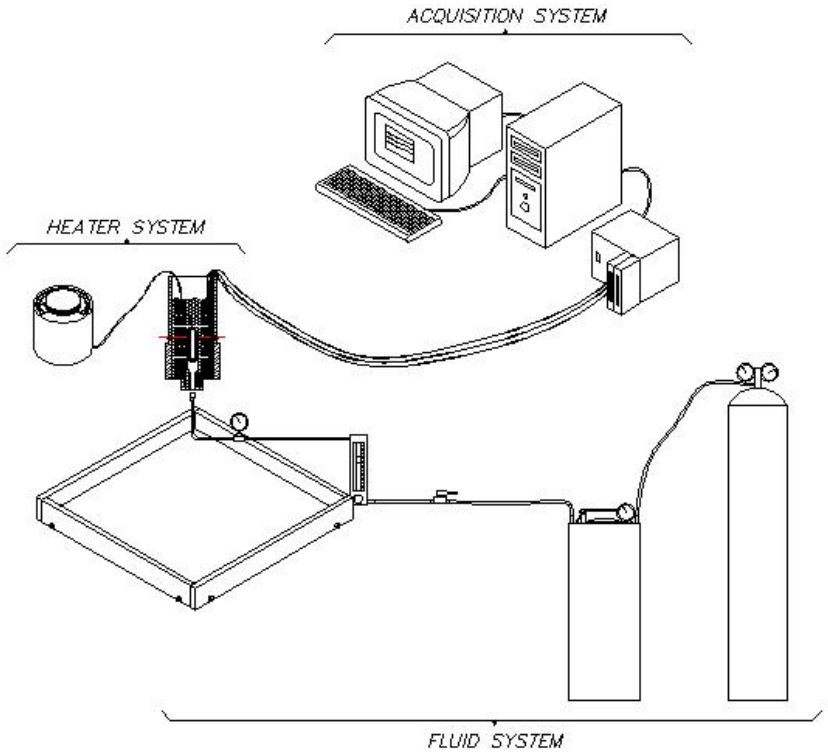

Figure 11: Schematic of Experimental Apparatus.

2.1 Experimental Apparatus

2.1.1 Fluid System

The fluid system (shown in Figure 12) consists of a high pressure nitrogen cylinder which provides pressure to a pressure tank. Due to pressurization of the tank, the working fluid is forced out of the pressure tank through the circuit.

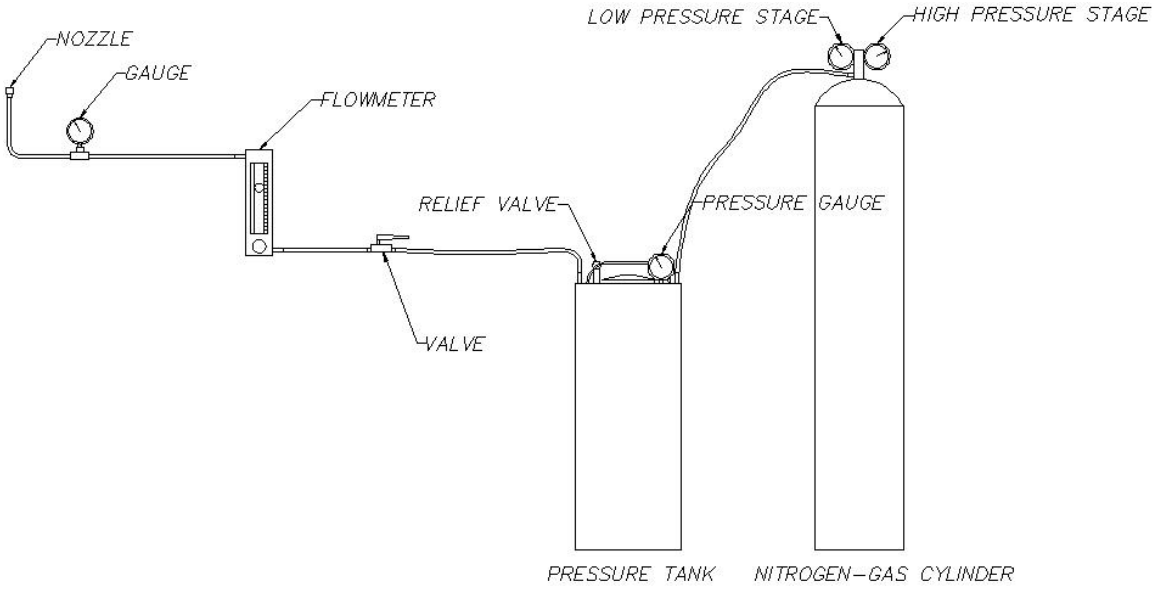

Figure 12: Schematic View of the Fluid System.

The flowmeter is used to control the volumetric flux and the pressure of the deionized water which is expelled through a nozzle. Water reaches the nozzle and exits as a high velocity spray.

The high-pressure nitrogen cylinder has a two-stage regulator valve which; first stage controls high pressure up to 3000 psi, and the second stage controls low pressure up to 200 psi. This two-stage regulator valve is used to provide constant pressure to the pressure tank, producing a constant flow rate during each experiment.

Figure 13: Two-Stage Regulator Valve.

A. Pressure Tank Specifications

The pressure tank is a dispensing pressure vessel made by Millipore Corporation which has the following specifications:

- Materials: Type 316L stainless steel with stainless fittings; Viton gaskets and O-rings; EPDM base.
- Pressure/Temperature: The maximum pressure allowed is 7 bars or 100 psi. and the maximum temperature allowed is 121 °C or 250 °F.
- Dimensions and Capacity: 229 mm diameter x 595 mm (9 in. x 23.44 in.); capacity: 20 liters.

Note: The pressure tank has a relief valve set for a pressure of 80 psi.

B. Pressure Gauges

Both pressure gauges, one in the pressure tank and the other just before the nozzle, can indicate pressures up to 160 psi or 11 kg/cm^2, in steps of 2 psi or 0.1 kg/cm^2 respectively.

C. Flow meter

The flow meter made by GILMONT Instruments has the following specifications:

- Float Material: Carboloy (14.98 g/ml)
- Max. & min. readings: 1866 ml/min & 176 ml/min respectively. (The tube has 13 scale readings).
- Pressure/Temperature: The maximum pressure allowed is 13.6 bars or 200 psi. and the maximum temperature allowed is 121°C or 250°F.

D. Nozzle

This is a full cone spray nozzle type “S” with the following specifications:

- Pipe size NPT: 1/8 “
- Pressure/Capacity: The maximum pressure allowed is 150 psi at which a flow rate of 0.39 GPM or 1478.1 ml/min is provided.

2.1.2 Heater System

The heater system (shown in Figure 14) consists of a cartridge holder (copper cylinder) which increases in temperature as the inserted heater is powered. The heater receives electric power via a variable autotransformer. The temperature gradient in the cartridge holder was measured using three thermocouples inserted into the copper cylinder; the first, 3 mm above the test surface; the second, 13 mm above the test surface and rotated 120° with respect to the first one; and the third, 23 mm above the surface and rotated 120° with respect to the second one.

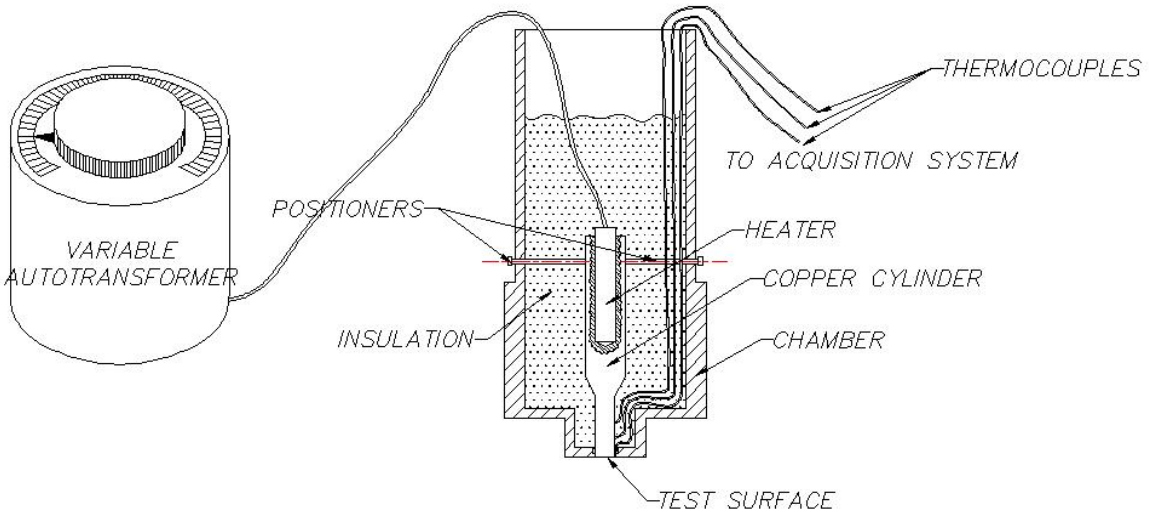

Figure 14: Schematic View of the Heater System.

A. Copper cylinder (or cartridge holder)

The copper cylinder consists of a 4 1/3" – long rod with two different diameters in its ends; the end into which the heater is inserted has a diameter of 1 " and the end which receives the spray has a diameter of 12 mm. The copper cylinder was fabricated in the Engineering machine shop of The University of South Florida and made for 99% pure copper bar stock. The end which receives the heater has a hole of 2 2/3" in length and 13 mm in diameter; and the holes which receive the thermocouples have a length of 6 mm and a diameter of 1 mm. The design and dimensions of the cartridge holder are shown in Figure 15.

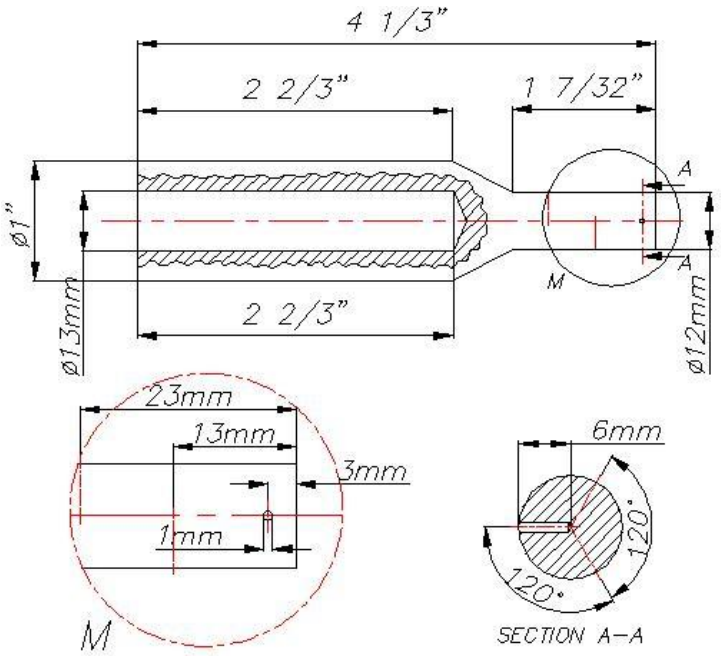

Figure 15: Copper Cylinder (Cartridge Holder).

B. Heater

The heater used in this experiment was made by *Chromalox* with 82 mm length and 12.5mm diameter. The heater was inserted into the copper cylinder and its cables were plugged into the variable autotransformer. It is rated for a maximum potential difference of 120 V and a maximum input power of 750 W.

C. Variable autotransformer

The variable autotransformer was made by *Staco Energy Products Co.*(shown in Figure 16) , and has the following characteristics:

- Input: Nominal (120 Volts), Line (50-60 Hz).
- Range: 0 - 140 (0 - 100%), in steps of 2.8 V or 2%.
- Max. Output: Constant Current Load (max. 10 Amps, max. 1.4 kVA)

Figure 16: Variable Autotransformer.

D. Thermocouples

Three precision, Type K, fine wire thermocouples made by *Omega* (0.010 ” in diameter and 72 ” in length) were used for the experiments. The thermocouples were used to measure the temperature gradient in the copper cylinder. Temperatures were monitored and recorded using an acquisition system to which the thermocouples were connected.

2.1.3 Acquisition System

The acquisition system consists of a desktop computer, an acquisition system made by *National Instruments (NI)*, and National Instruments LabView 7.1 (shown in Figure 17). The acquisition system has a terminal block for up to 31 channels (shown in Figure 18). The data obtained from the acquisition system was displayed on the computer monitor and recorded in files using LabView.

A. Acquisition system

The acquisition system consists of a PCI card which was installed on the motherboard of the computer. This card is connected via cable with the SCXI - 1000 or signal conditioning. Finally, the thermocouples are connected to the SCXI via a terminal block (SCXI - 1303), shown in Figure 17.

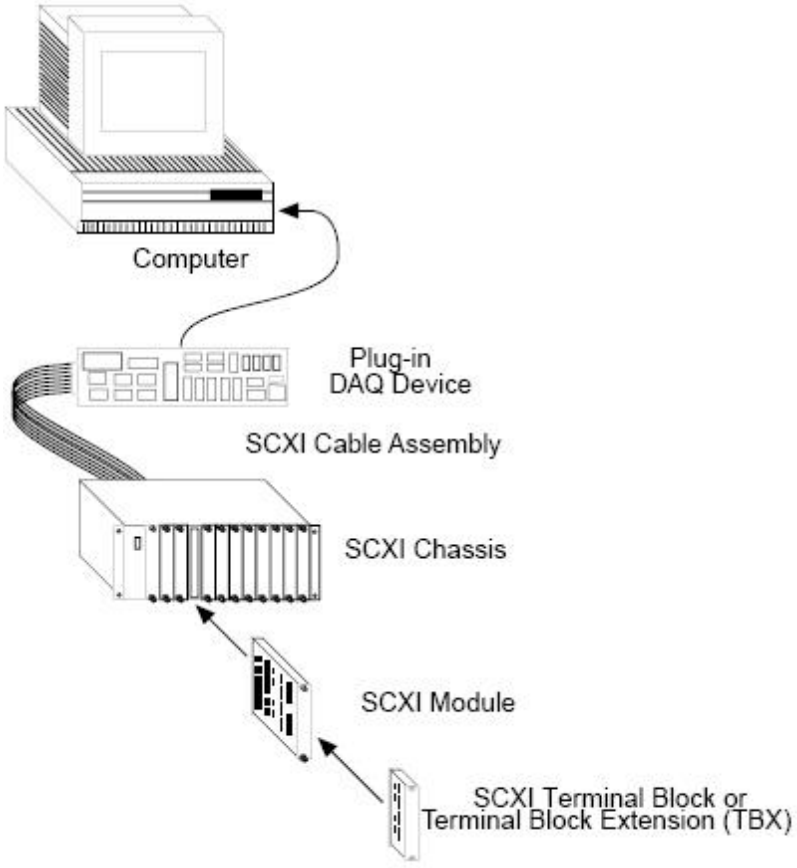

Figure 17: SCXI System Components (National Instruments).

The thermocouples were connected to the terminal block (SCXI - 1303) as shown in figure 18.

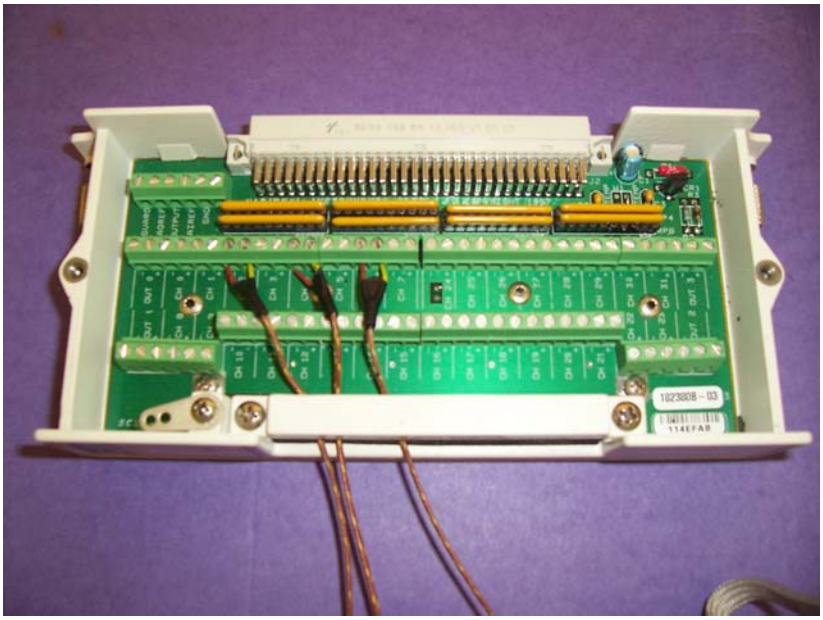

Figure 18: Installation of Thermocouples in the Terminal Block (SCXI-1303).

B. Computer

The computer has an Intel Pentium III Processor with 663 MHz and 256 MB of RAM.

C. Acquisition Software

Labview is a software tool for designing test, measurement, and control systems. This software analyzes real-time signals and shares the results via output-data devices like computer screen, printer, etc. In this experiment, the LabView program showed the temperatures indicated by the thermocouples on the computer screen, and recorded the temperatures in electronic format.

The acquisition system was configured to read 1 sample in a rate of 10 Hz. Thus, the program displays 1 set of data (for three thermocouples) in the chart every 0.1 seconds; or 10 sets every second. This resolution is good enough to obtain an acceptable measure of the transient temperatures.

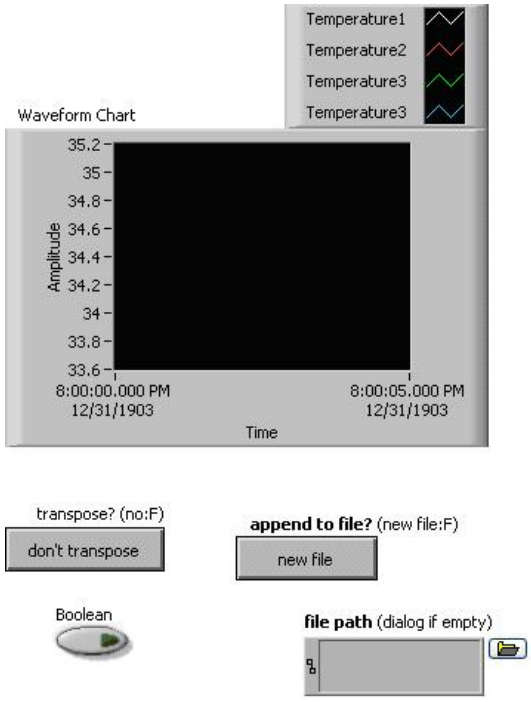

Figure 19: Front Panel Designed for the Experiment.

2.2 Operating Procedure

The operating procedure involved the following steps:

A. Verification of the equipment

At the beginning of the experiment, the pressure in the nitrogen cylinder and in the pressure tank were verified to be 0 psi, and at the same time, the input power from the variable autotransformer was verified to be 0 W. All the cables from the heater system as well as the hoses and connections from the fluid system were verified to prevent a short-circuit or a possible reduction of the fluid pressure due to rundowns. Other verifications involved: distance between the nozzle and the test surface, functioning of the acquisition system, etc.

B. Operating Procedure

After the pressure tank was filled with deonized water, it was pressurized with nitrogen from the nitrogen cylinder. The valve between the flowmeter and the pressure tank was maintained closed until the activation of the heated system. After the fluid system was ready, the input power from the variable autotransformer was increased in steps of 5% from 5% to 80% (1.5 to 628.6 W). The temperatures indicated by the thermocouples inserted into the copper cylinder increased soon after the increment of the input power. The fluid system was activated as soon as the temperature reached a certain level. The volumetric flow rate was controlled using a flowmeter between the nozzle and the pressure tank (336.6 to 627 ml/min). When the temperatures reached steady-state, after 4 - 5 minutes approximately, the temperatures were recorded for 12 seconds approximately (50 data).

Once the data were recorded, the input power was increased by 5% and the procedure was repeated. Because there was a limited amount of deionized water in the pressure tank, it was important to leave some water in order to cool the test surface. When the maximum of the three temperatures reached 35 °C, the fluid system was stopped and the pressure tank was refilled with deonized water.

C. Maintenance

During the experiment, some equipment needed to be maintained. They included the copper cylinder, variable autotransformer, and flowmeter. The copper cylinder oxidized when it was used at high input power levels. Thus, its

surface was cleaned regularly. At very high heat fluxes, there is always risk of the electric cables being short-circuited. Thus, it was occasionally necessary to change the fuse in the variable autotransformer. Finally, filling the pressure tank sometimes introduced solids into the fluid system that became stuck in the filter of the flowmeter. Thus, the filter and the flowmeter were cleaned occasionally.

2.3 Experimental Parameters

2.3.1 Distance between Test Surface and Nozzle

The distance between the nozzle and the test surface is directly related to the sprayed area and the volumetric flow rate. Thus, this parameter affects the heat transfer performance. Because of that; many researchers have studied its affects on spray cooling systems. In the case when the nozzle is very near the test surface, the sprayed area become very small and in the case when the nozzle is very far from the test surface, part of the liquid is sprayed off the test surface, thus there is a reduction of the volumetric flow rate (as shown in Figures 20 and 21).

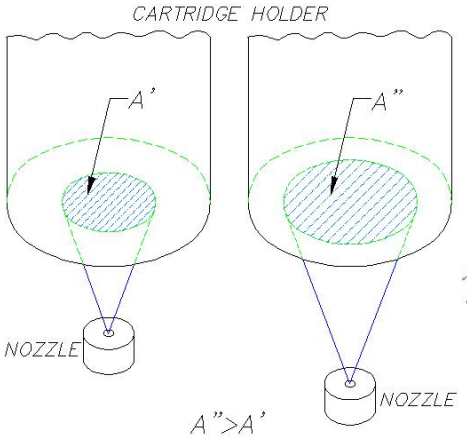

Figure 20: Distance (H) Affecting the Sprayed Area.

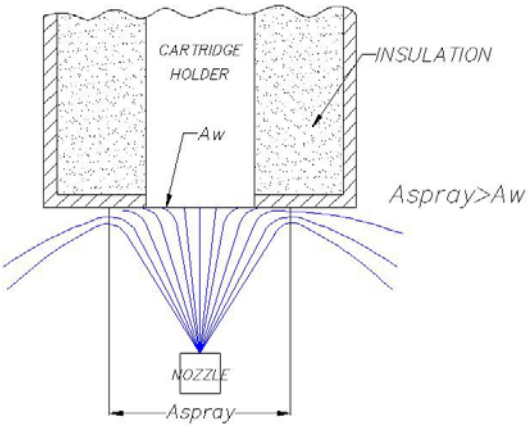

Figure 21: Distance (H) Affecting the Volumetric Flow Rate.

Fabbri, M & Dhir, V. K. [11], studied the effect of an orifice plate to heater distance (H) on the heat transfer rate, using FC 40 as a test liquid and flowrates from 240 ml/min [13.67 $\mu l/mm^2$ s] to 410 ml/min [23.36 $\mu l/mm^2$ s]. The spray distance was varied from 10 mm to 2.1 mm, which corresponds to a range of H/d_n (ratio between the distance orifice-heater and jet's diameter) between 12.1 and 57.6. The results show that for high Reynolds number (500, high velocity of spray) and for increments of H/dn(increment of the distance H), there is an increment in Nusselt number; but for small Reynolds number (300), there is no change in Nusselt number. This means that for high velocity of the spray, we can obtain higher rate of heat transfer using higher H, but only until a certain distance due to the hydrodynamic instability of the spray.

Another study made by Wang, G. X., et al. [42] in CSC shows that the spray distance has a high effect on the temperature of the skin. For H between 15 – 40 mm, the temperature of the skin was maintained more time at low temperature for high distances; but for H between 40 – 80 mm, the results were opposite, thus the distance which had the maximum deposition of cryogen droplets was H = 40 mm.

In the present study, the distance between the nozzle and the test surface were: 3 mm, 7 mm and 12 mm. In each case, the total volumetric flow rate was varied from 336.6 ml/min to 627 ml/min; but for the case of H = 12 mm, part of the fluid did not impinge to the test surface (see Table 1, subchapter 3.3).

2.3.2 Volumetric Flow Rate

The volumetric flow rate and the temperature of the working fluid are definitely the parameters which affect most the heat transfer during spray cooling. Both parameters have been studied by many researchers and the results of their studies are in agreement.

In the present investigation, the total volumetric flow rates were: 336.6, 464.6, 523.8, 583, and 627 ml/min, which were obtained by varying the nozzle pressure: 10, 15, 20, 25, 30 psi respectively. The volumetric flow rate impacting the surface area depended on the nozzle - test surface distance and the pressure. For very large distances and high pressures, some liquid did not impinge the test surface, thus the volumetric flow rate was reduced by 7.54% (for H = 12 mm, P = 20 psi); and by 24.38% (for H = 12 mm, P = 25 psi; and H = 12 mm, P = 30 psi).

Chapter Three - Experimental Results

3.1 Heat Flux and Temperature of Surface Calculation

In this study, the heat flux depended on the temperature difference between the thermocouples embedded in the cartridge holder, the distance between the thermocouples, and the thermal conductivity of the cartridge holder (see also Chapter 1).

The heat flux was calculated using equation (3). An example of the calculation for the case where the heat flux along points (1)-(2) was greater than points (2)-(3), and for the case where H = 7 mm, IP = 247.2 W and the V” = 336.6 ml/min is shown in Appendix A.

The results for the heat flux and the temperature of the heated surface for all the cases are shown in Appendix B.

3.2 Heat Transfer Coefficient Calculation

In this study, the heat transfer coefficient depended on the heat flux, the surface temperature calculated in 3.1, and the temperature of the fluid which is 20.5 °C. An example of heat transfer coefficient calculation for H = 3mm, V” = 336.6 ml/min and IP = 163.5 W is shown in Appendix C. The results of the heat transfer coefficient for all the cases are shown in Appendix D.

Many researchers use the curve heat transfer coefficient (h) versus heat flux (q") as a way to determine the spray cooling performance. Figures 22, 23 and 24, show the heat transfer coefficient versus heat flux for different volumetric flow rates at H = 3 mm, 7 mm and 12 mm respectively.

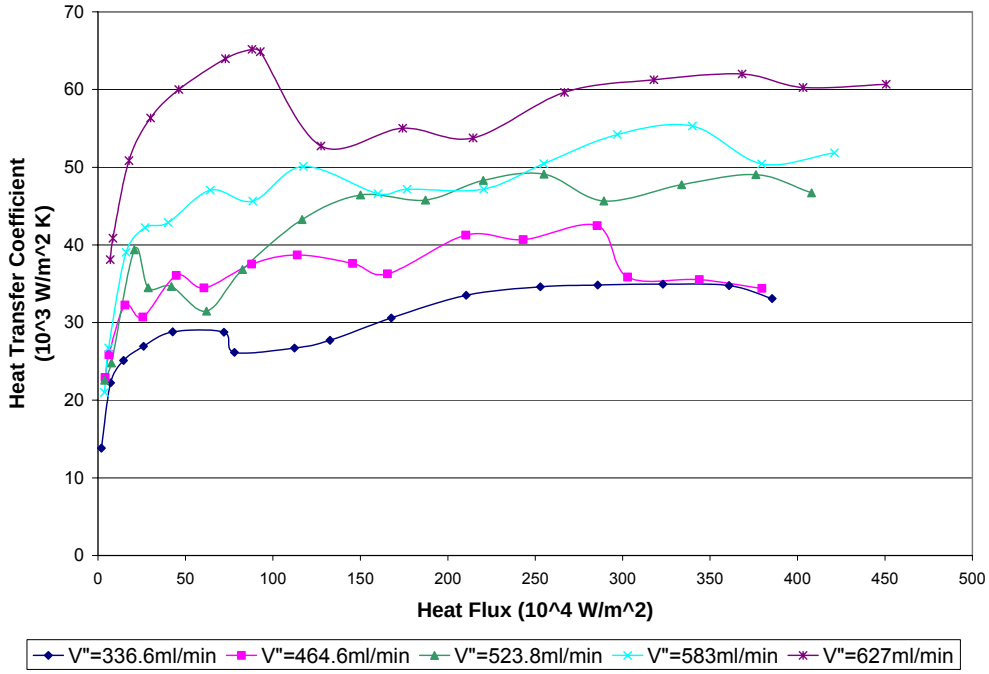

Figure 22: Heat Transfer Coefficient Vs Heat Flux for Different Volumetric Flow Rate at H = 3 mm.

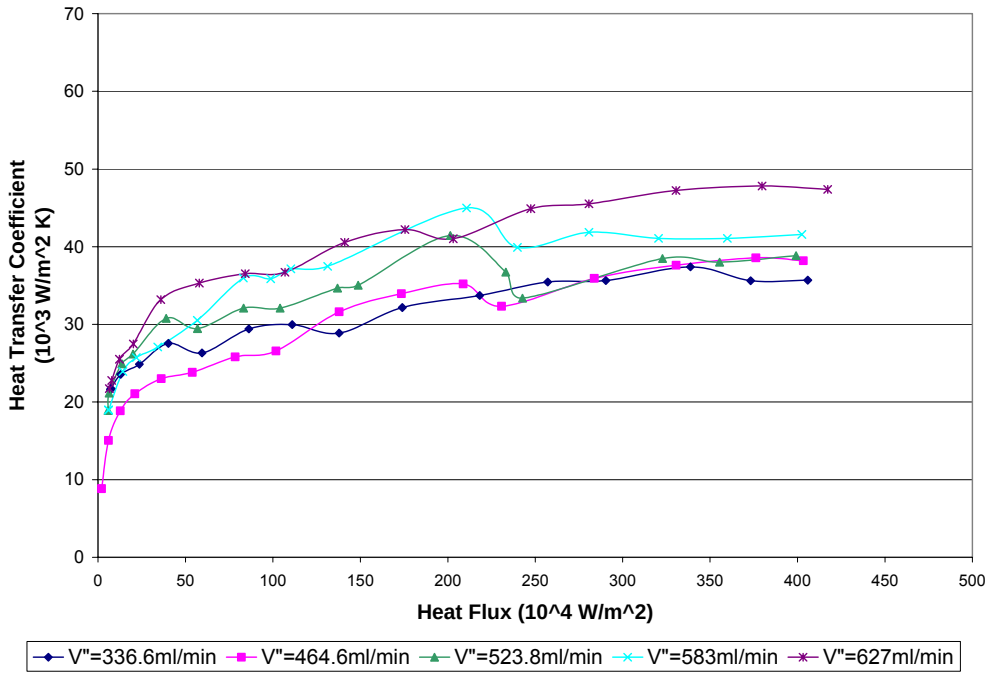

Figure 23: Heat Transfer Coefficient Vs Heat Flux for Different Volumetric Flow Rate at H = 7 mm.

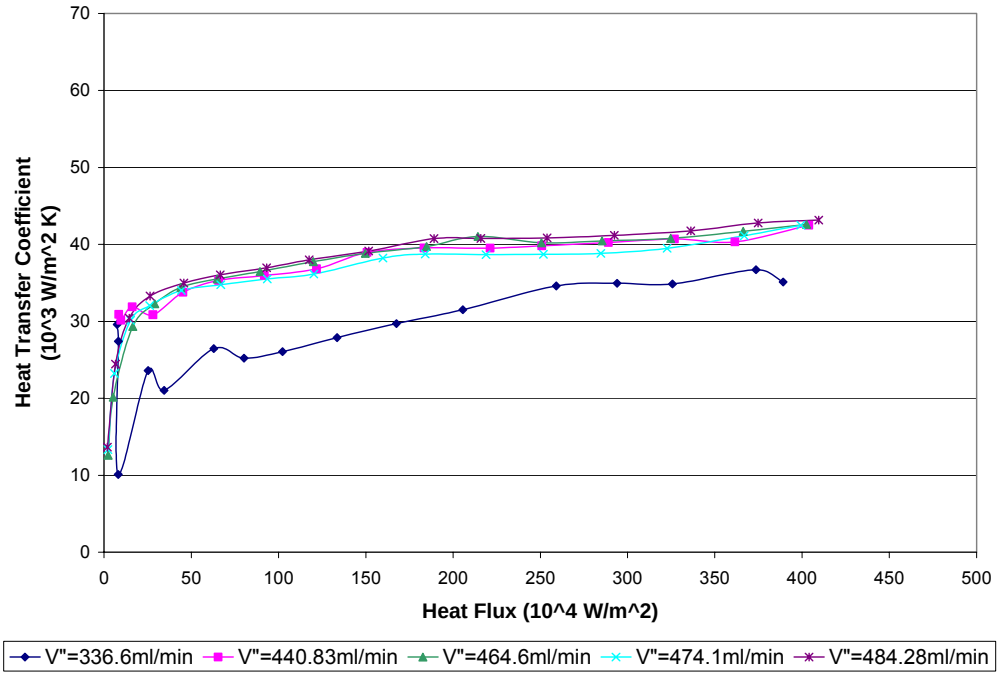

Figure 24: Heat Transfer Coefficient Vs Heat Flux for Different Volumetric Flow Rate at H = 12 mm.

3.3 Volumetric Flow Rate Calculation

In the present study, 5 different pressures (10, 15, 20, 25 and 30 psi) were used producing different volumetric flow rates at three distances (H = 3, 7 and 12 mm). This volumetric flow rate impacting the test surface (V") was different from the total volumetric flow rate ($V"_T$) for the case of H = 12 mm and pressures over 20 psi. At high pressures, the angle of the spray became greater and consequently the spray area became greater than the test surface area.

An example for the calculation of the volumetric flow rate is shown in Appendix E.

For the case when $A_w > A_{spray}$, the volumetric flow rate on the test surface was the same as the total volumetric flow rate ($V" = V"_T$). The next table shows the volumetric flow rate on the test surface for different pressures (P) and distances (H).

Table 1: Volumetric Flow Rate on the Test Surface in (ml/min) for Different Pressures and Distance between the Test Surface and the Nozzle.

Pressure (psi) H(mm)	10	15	20	25	30
3	336.6	464.6	523.8	583	627
7	336.6	464.6	523.8	583	627
12	336.6	464.6	484.28	440.83	474.1

3.4 Uncertainty and Error Calculations

In the present investigation, uncertainties for heat flux, and volumetric flow rate were calculated. The uncertainty of the heat flux depends on the uncertainty of the distance between two levels of thermocouples, the temperature difference between two consecutive points, and the variation of the thermal conductivity of

the copper cylinder. The uncertainty of the volumetric flow rate depends on the uncertainty of the flowmeter, the uncertainty of the ratio between the sprayed area and the test area, and the uncertainty of the distance between the nozzle and the test surface.

3.4.1 Heat-Flux Uncertainty Calculation

In this study, the uncertainty of heat flux ($U_{q"}$) depended on the uncertainty of the following parameters: measured temperature difference ($U_{\Delta T}$), the spatial separation ($U_{\Delta x}$) and the thermal conductivity of the copper cylinder (U_{KCu}).

Beckwith, 1990 and Holman, 1989 suggested the following equation to measure the uncertainty of heat flux:

$$\frac{U_{q"}}{q"} = \left[\left(\frac{U_K}{K_{Cu}}\right)^2 + \left(\frac{U_{\Delta T}}{\Delta T}\right)^2 + \left(\frac{U_{\Delta X}}{\Delta X}\right)^2 \right]^{1/2} \qquad (16)$$

A. Temperature Difference Uncertainty Calculation ($U_{\Delta T}$)

In the case of the measured temperatures, it is very important to recall that the uncertainty is on the difference (ΔT) of the temperatures and not only on one temperature. This uncertainty can be calculated using equation (13):

$$U_{\Delta T}^2 = U_{T1}^2 + U_{T2}^2 \qquad (17)$$

Where: U_{T1} and U_{T2} are the uncertainties of thermocouple at distances (1) and (2).

The uncertainty for both thermocouples is the same due to the fact that only one type of thermocouple (Type K), and only one acquisition system were used. In this particular case, $U_{T1} = U_{T2} = 0.001$ °C.

Then, replacing in equation (17):

$$U_{\Delta T}^2 = 0.001^2 + 0.001^2$$

$$\rightarrow U_{\Delta T} = 0.0014\ °C$$

B. Uncertainty Spatial Separation Calculation ($U_{\Delta x}$)

In the case of the spatial separation (Δ_X), the diameter of the thermocouples was slightly shorter than the diameter of the holes. This produced an uncertainty about the distance from one thermocouple to another (shown in Figure25).

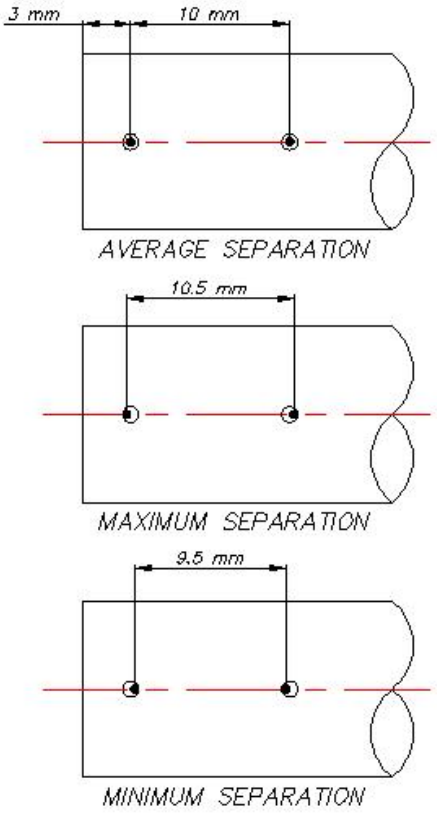

Figure 25: Uncertainty of the Spatial Separation between Thermocouples.

The uncertainty can be expressed as the difference between the maximum/minimum and the average separation:

$$\rightarrow U_{\Delta X} = (10.5 - 10) = \pm 0.5\ mm$$

C. Uncertainty Thermal Conductivity of the Cartridge Holder Calculation (U_{KCu})

A thermal conductivity of 400 W/m K was used to calculate the heat flux, which varied less than 13 W/m K over the temperature range reported in the results (JAHM Software, Inc. [43], see Figure 26).

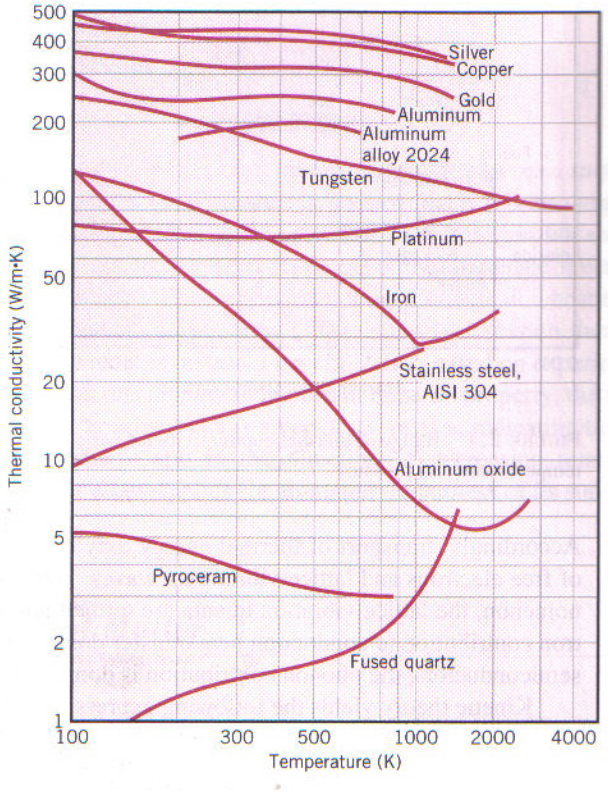

Figure 26: The Temperature Dependence of the Thermal Conductivity of Selected Solids [44].

Then the uncertainty of the thermal conductivity of the cartridge holder can be expressed as:

$$\rightarrow U_{KCu} = 13\ W/m\ K$$

In order to calculate the uncertainty of the heat flux, the following quantities were used:

- q" = 1742160 W/m^2 (for the case of 3 mm_627 ml/min_50%)
- ΔT = 35.7 °C (temperature difference between points 2 and 3 (see Figure 10) for the same case)
- Δx = 10 mm
- K_{Cu} = 400 W/m K
- $U_{\Delta T}$ = 0.0014 °C
- $U_{\Delta X}$ = $\pm$ 0.5 mm
- U_{KCu} = 13 W/m K

Using all these quantities, the uncertainty of the reported heat flux was calculated using equation (16):

$$U_{q''} = 1742160\ W/m^2 \left[\left(\frac{13}{400}\right)^2 + \left(\frac{0.0014}{35.7}\right)^2 + \left(\frac{0.5}{10}\right)^2 \right]^{1/2}$$

$$U_{q''} = 103888.87\ W/m^2 \text{ or } \frac{U_{q''}}{q''} = 5.9\%$$

3.4.2 Volumetric Flow Rate Uncertainty Calculation

The uncertainties were obtained experimentally and by calculation. The total volumetric flux (the maximum volumetric flux the nozzle gives to the test surface) was measured experimentally using a flow meter (see subchapter 2.1.1). Figure 27 shows the relation between the pressure and the total volumetric flux.

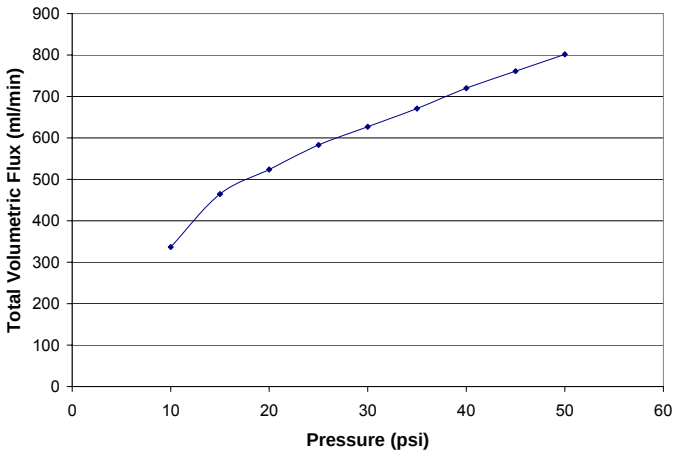

Figure 27: Relation between Pressure and Total Volumetric Flux.

This curve can be considered linear from 15 to 50 psi, and then the uncertainty of the flow meter can be obtained from this calculation:

Using the flow meter calibration data, the flow for a scale reading of 35 is 987 ml/min; and for 30 is 829 ml/min. Interpolating these two data, the flow for a scale reading of 34 is 955.4 ml/min.

The minimum volumetric flux the equipment can read is:

$$987\text{-}955.4 = 31.6 \text{ ml/min}$$

Then, the uncertainty of the flow meter is half of the minimum reading:

$$31.6 / 2 = \pm 15.8 \text{ ml/min}$$

Table 2: Relation between Pressure and Total Volumetric Flux.

Pressure (psi)	Flow scale	Flow rate (ml/min)	Uncertainty (ml/min)
10	11	336.6	
15	16	464.6	
20	18	523.8	
25	20	583	
30	22	627	+/- 15.8
35	24	671	
40	26	720.2	
45	27.5	761	
50	29	801.8	

The test surface received in some cases only a fraction of this total volumetric flux (shown in Figure 21). The fraction of the test surface area with the maximum spray area defined the uncertainty of the volumetric flux used in the experiments.

The spray area depends on the nozzle pressure. In this experiment, between 10 to 30 psi, the angle of the spray increased between 35° to 60° with an uncertainty of +/- 2.5° (see Table 3).

Table 3: Relation between Pressure and Spray Angle.

Pressure (psi)	Spray Angle (º)	Uncertainty (º)
10	35	+/- 2.5
15	45	
20	55	
25	60	
30	60	

The spray area is not only related to the spray angle but also to the distance between the nozzle and the test surface. If the nozzle is very close to the test surface, all the fluid will impinge it. If the nozzle is far from the test surface, then only part of the fluid will impinge it. Table 4 shows the ratio between the theoretical coverage (W) and the distance (H) from the nozzle to the test surface for many spray angles.

Table 4: Ratio between the Theoretical Coverage (W) and Distance (H) at Various Spray Angles.

INCLUDED SPRAY ANGLE (º)	5	10	15	20	25	30	35
W/H RATIO	0.087	0.175	0.263	0.353	0.443	0.536	0.631
INCLUDED SPRAY ANGLE (º)	40	45	50	55	60	65	70
W/H RATIO	0.728	0.828	0.933	1.04	1.15	1.27	1.4

The nozzle pressure was high enough to assure that the fluid would impinge the test surface. This assertion is demonstrated by the ratio between the nozzle pressure and the distance between the nozzle and the test surface (H) as shown in Table 5.

Table 5: Relationship of the Pressure Head at the Nozzle to the Distance (H).

(psi)	mmH2O	DISTANCE		
		3 mm	7 mm	12 mm
10	7040.97	2347	1006	587
15	10561.46	3521	1509	880
20	14081.95	4694	2012	1174
25	17602.43	5868	2515	1467
30	21122.92	7041	3018	1760

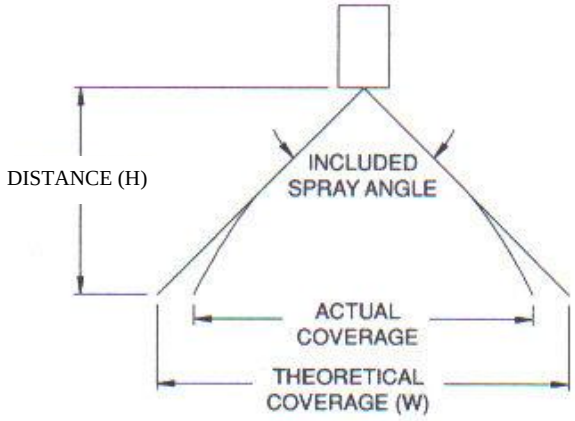

Figure 28: Spray Coverage (from BEX SPRAY NOZZLES, Catalog N°52).

In this study, the actual coverage and theoretical coverage (W), shown in Figure 28, are considered similar because the distance (H) is very small. The nozzle, used in this study, is a commercial nozzle which is commonly used for larger distances (H), necessitating differentiation of actual and theoretical coverage. Thus, the difference between the actual and theoretical coverage is negligible for the small distances used in the present investigation.

Using the ratio (r=W/H) it is very easy to calculate the uncertainties for the area (A_{spray})of the spray using the formulas given before:

$$A_{spray} = \frac{\pi \times [r \times H]^2}{4}$$

Where r is the ratio given in Table 4, and H is the distance between the nozzle and the test surface in mm. The most critical case is with the highest ratio and highest distance (H), as we can see in the next calculation:

$$A_{spray} = C \times r^2 \times H^2 \qquad (18)$$

Where C is a constant = 0.7854

Calculation of uncertainty (using the equations given before):

$$\frac{U_{Aspray}}{A_{spray}} = 2 \times \frac{U_r}{r} + 2 \times \frac{U_H}{H}$$

Then:
$$U_{Aspray} = A_{spray} \times \left[2 \times \frac{U_r}{r} + 2 \times \frac{U_H}{H}\right] \qquad (19)$$

Replacing (18) in (19):

$$U_{Aspray} = C \times r^2 \times H^2 \times 2 \times \frac{U_r}{r} + C \times r^2 \times H^2 \times 2 \times \frac{U_H}{H}$$

$$\rightarrow U_{Aspray} = 2 \times C \times r \times H \times [H \times U_r + r \times U_H]$$

Here, we can see the critical case is for r maximum and H maximum. The uncertainty (U_r) has to be calculated because it depends on the spray angle which has an uncertainty of $\pm$ 2.5°.

Using Table 4 and interpolations, the following results were obtained:

Table 6: Maximum and Minimum Ratios for a Spray Angle of 60°.

INCLUDED SPRAY ANGLE (°)	55	57.5	60	62.5	65
W/H RATIO	1.04	1.095	1.15	1.21	1.27

From Table 6, we can calculate the uncertainty: 1.21 – 1.15 = 0.06 or 1.15-1.095 = 0.055. Thus, the uncertainty is +/- 0.06.

Finally, using H = 7 mm, and U_H = 0.5 mm (Uncertainty of a ruler), the uncertainty of the sprayed area is:

$$U_{Aspray} = 2 \times 0.7854 \times 1.15 \times 7\ mm \times [7\ mm \times 0.06 + 1.15 \times 0.5\ mm]$$

$$\rightarrow U_{Aspray} = \pm 12.58\ mm^2$$

As it was recalled before, the volumetric flow rate impacting the test surface is only a fraction of the total volumetric flux rate. If the flux is considered uniform in the spray, then the volumetric flow rate can be obtained as follows:

$$V'' = V''_T \times \frac{A_w}{A_{spray}} \qquad (20)$$

Before calculating the uncertainty of the volumetric flow rate on the test surface, it is very important to calculate the uncertainty of the area of the test surface:

$$A_w = \frac{\pi \times \Phi^2}{4} = C \times \Phi^2$$

Where: Φ = 12 mm (diameter of the test surface).

Then, using the equations presented before:

$$U_{Aw} = 2 \times C \times \Phi \times U\Phi$$

Where: C = 0.7854

U_{Φ} = 0.01 mm (uncertainty of caliper)

Replacing: $U_{Aw} = 2 \times 0.7854 \times 12\ mm \times 0.01\ mm = 0.19\ mm^2$.

Finally, the uncertainty of the volumetric flux rate for the test surface can be calculated as follows:

$$U_{V''} = V'' \left[\frac{U_{V''T}}{V''_T} + \frac{U_{Aw}}{A_w} + \frac{U_{Aspray}}{A_{spray}} \right] \qquad (21)$$

Where: $U_{V''T}$ = 15.8 ml/min, uncertainty of the total volumetric flux (from Table 2).

U_{Aspray} = 12.58 mm^2

U_{Aw} = 0.19 mm^2

$A_w = \pi \times (12\ mm)^2 / 4 = 113.1\ mm^2$

Replacing (20) in (21), we obtain:

$$U_{V''} = \frac{A_w \times U_{V''T}}{A_{spray}} + \frac{V_T \times U_{Aw}}{A_{spray}} + \frac{V_T \times A_w \times U_{Aspray}}{A_{spray}^2}$$

The uncertainty of the volumetric flow rate for the test surface ($U_{V''}$) is critical with a maximum total volumetric flux rate (V''_T) and a minimal sprayed area (A_{spray}). This condition produces an invalid uncertainty, as we can see in the next example:

Using: Maximum total volumetric flux rate, V''_T = 627 ml/min from Table 2.

Minimal sprayed area, $A_{spray} = \frac{\pi \times [0.63 \times 3mm]^2}{4} = 2.8mm^2$

The uncertainty is:

$$U_{V''} = \frac{113.1\ mm^{2x}\ 15.8\ ml/min}{2.8\ mm^2} + \frac{627\ ml/min \times 0.19\ mm^2}{2.8\ mm^2} +$$

$$\frac{627\ ml/min \times 113.1\ mm^2 \times 12.58\ mm^2}{(2.8\ mm^2)^2} = 114468.29\ ml/min$$

The error in the calculation of the uncertainty is due mainly of the bad assumption that the test surface can receive more than the total volumetric flux. This explanation can be seen clearly in this equation:

$$V'' = V''_T \times \frac{A_w}{A_{spray}}$$

This equation has been used to calculate the volumetric flux rate for the test surface (V"). If we insert all the parameters that have been used to calculate $U_{V"}$, we will obtain an incredible high V".

$$V'' = \frac{627\ ml/min \times 113.1\ mm^2}{2.8\ mm^2} = 25326.32\ ml/min$$

Explanation: The equation to obtain V" is only valid when the sprayed area (A_{spray}) is equal or greater than the area of the test surface (A_w). If A_W is greater than A_{spray}, then the volumetric flow rate on the test surface is equal to the total flow rate. This means that the uncertainty for the case when all the fluid impinge the test surface is the same as the uncertainty for the total volumetric flux rate ($U_{V"T}$ = 15.8 ml/min); but for the case when part of the fluid impinges on the test surface, the uncertainty involves the ratio between A_w and A_{spray}, and the critical condition is when the A_w/A_{spray} = 1.

Then, reevaluating the uncertainty:

$$U_{V''} = \frac{113.1\ mm^{2x}}{113.1\ mm^2} \frac{15.8\ ml/min}{} + \frac{627\ ml/min \times 0.19\ mm^2}{113.1\ mm^2} +$$

$$\frac{627 \text{ ml/min} \times 113.1 \text{ mm}^2 \times 12.58 \text{ mm}^2}{(113.1 \text{ mm}^2)^2} = 86.59 \text{ ml/min}$$

In this study, there were only three cases in which A_{spray} was greater than A_w, for the distance between the nozzle and the test surface of 12 mm and at 20, 25 and 30 psi of pressure. The error in percentage in each case is less than 20%:

- For 12 mm and 20 psi:

  V" = 484.28 ± 86.59 ml/min or 484.28 ± 17.88%

- For 12 mm and 25 psi:

  V" = 440.83 ± 86.59 ml/min or 440.83 ± 19.64%

- For 12 mm and 30 psi:

  V" = 474.1 ± 86.59 ml/min or 474.1 ± 18.26%

The conclusion from all these calculations is that even though critical parameters were used, the uncertainty of the volumetric flux rate on the test surface was relatively low (86.59 ml/min or less than 20% in percentage error).

3.5 Heat Transfer Curves

Many researchers use heat transfer curves in order to demonstrate how different parameters affect the heat transfer characteristics. Heat transfer curves usually show heat fluxes versus the temperature difference between the heated surface and the temperature of the working fluid ($T_w - T_f$), or versus the difference between the heated surface and the saturation temperature of the fluid ($T_w - T_{sat}$). For this study, the temperature of the fluid (Tf = 20.5 °C) was used

instead of the saturation temperature of the fluid. Figures 29, 30 and 31 show the heat transfer curves for different volumetric flow rate at different H.

Error bars, based on uncertainty analysis results, are included in the graphs. In Figure 30, the heat fluxes for volumetric flow rates of 336.6, 464.6, and 523.8 ml/min are the same when considering the uncertainty of the results according to the displayed error bars. Also, because of the uncertainty of the results, in Figure 31, the heat fluxes for volumetric flow rates of 440.83, 464.6, 474.1, and 484.28 ml/min are the same. In Figure 32, the heat fluxes for the three distances (3, 7, and 12 mm) are the same; and in Figure 35, the heat fluxes for the volumetric flow rate of 583 ml/min and distance of 7mm are the same as for the volumetric flow rate of 440.83 ml/min and distance of 12mm.

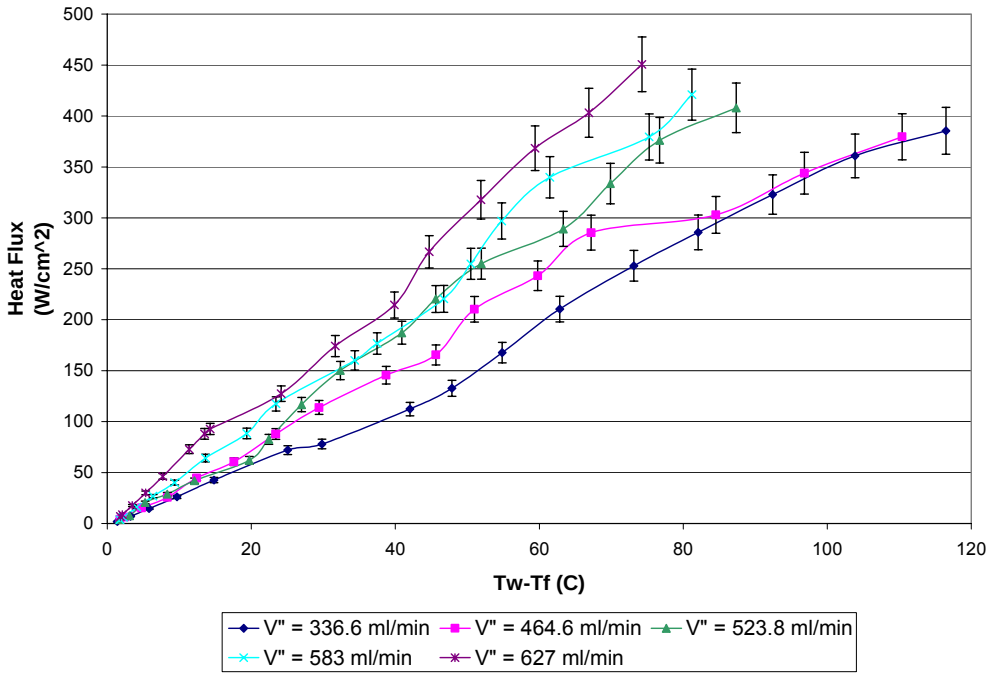

Figure 29: Heat Transfer Curve for H = 3mm and Different Volumetric Flow Rates.

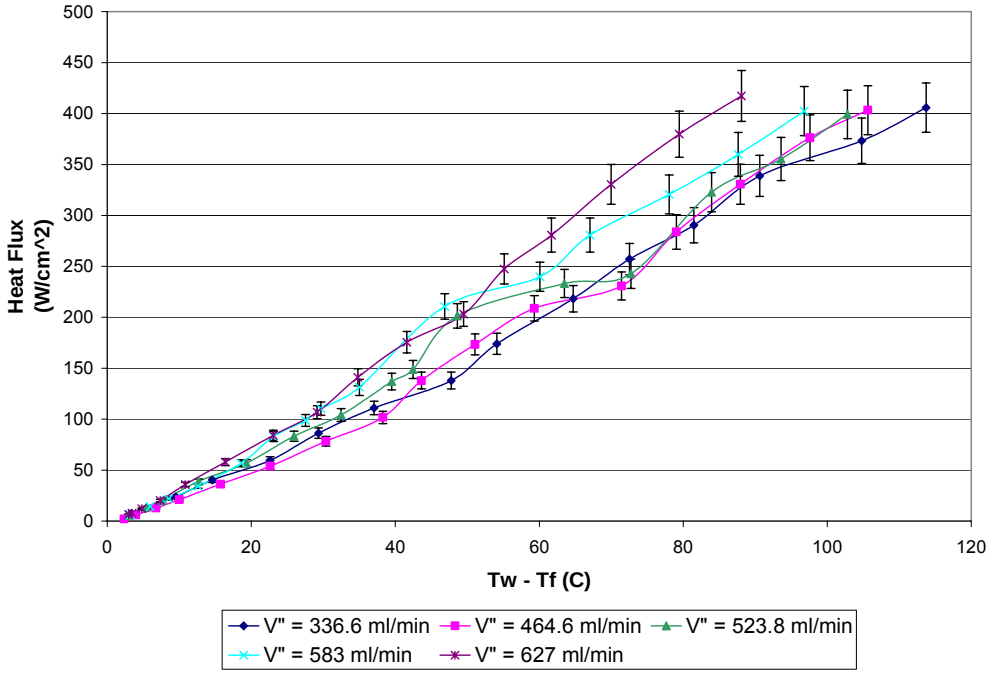

Figure 30: Heat Transfer Curve for H = 7 mm and Different Volumetric Flow Rates.

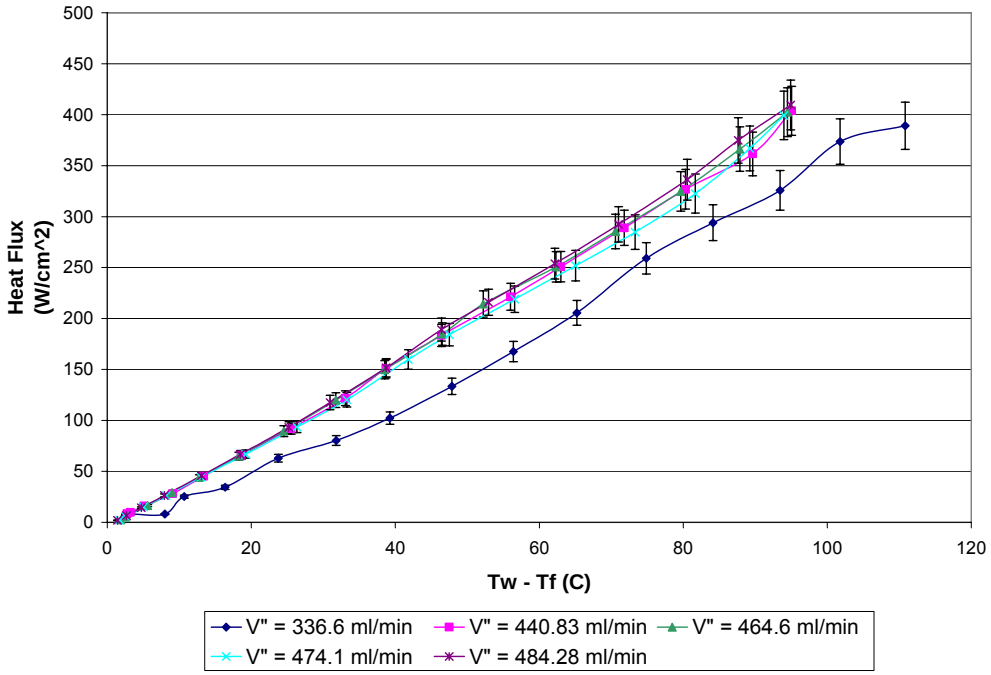

Figure 31: Heat Transfer Curve for H = 12 mm and Different Volumetric Flow Rates.

Figures 32 and 33 show the heat transfer curves for different H, at volumetric flow rate of 336.6 ml/min and 464.6 ml/min respectively.

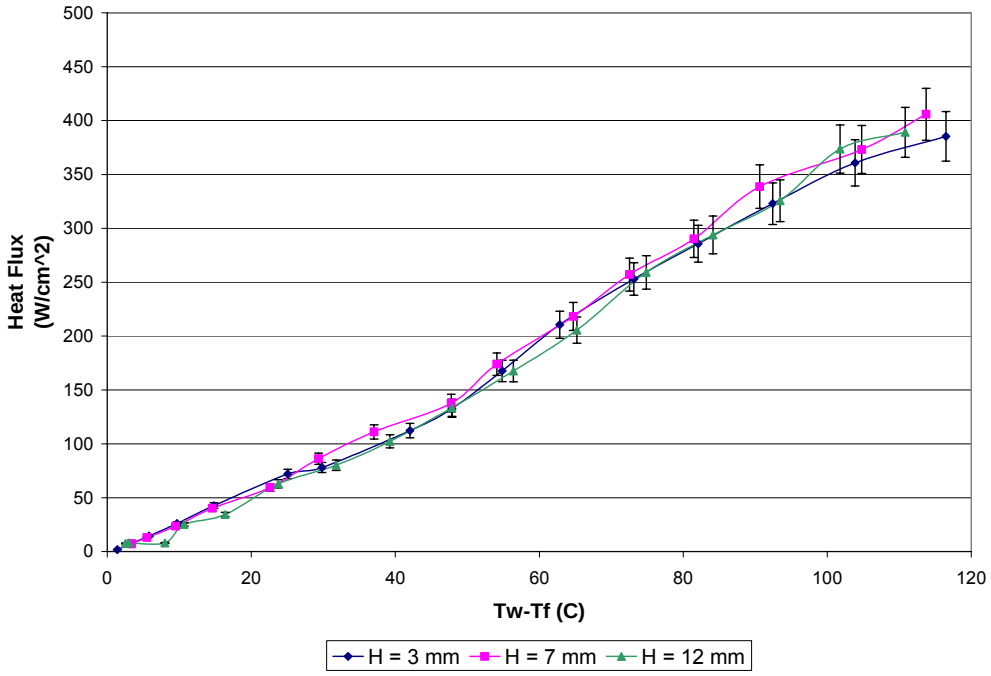

Figure 32: Heat Transfer Curve for V" = 336.6 ml/min and Different H.

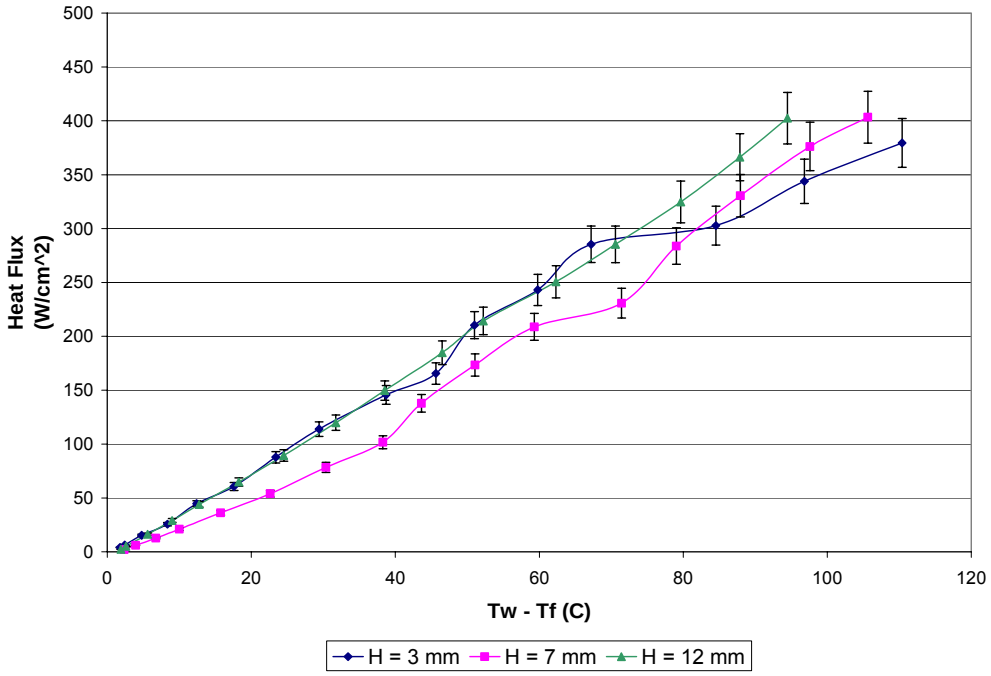

Figure 33: Heat Transfer Curve for V" = 464.6 ml/min and Different H.

Figures 34 - 36 show how the reduction of the volumetric flow rate affects the heat flux.

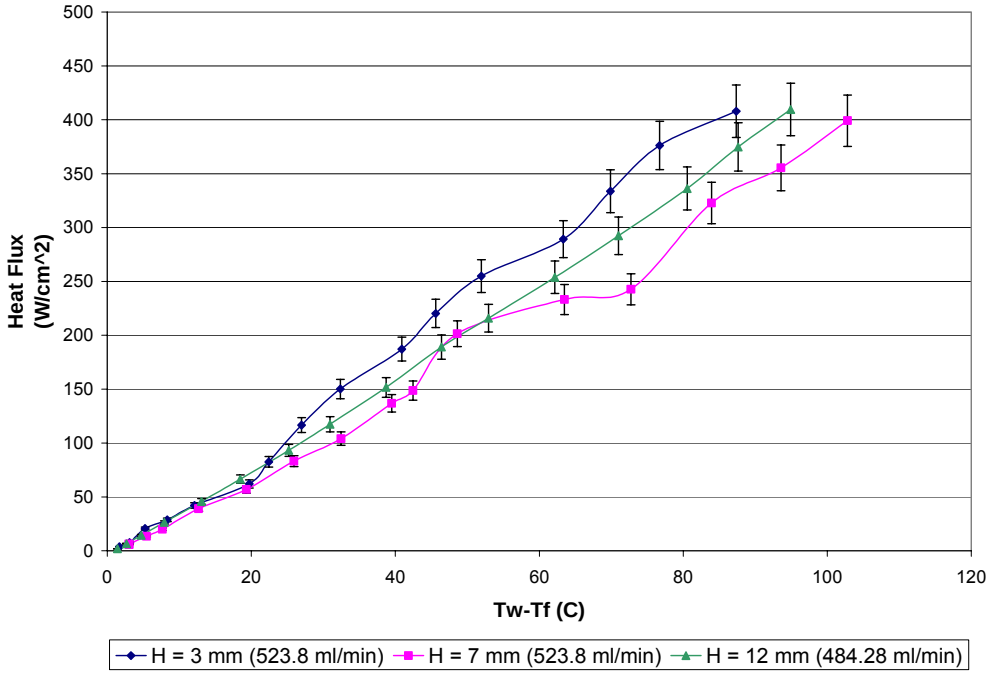

Figure 34: Heat Transfer Curve for P=20 psi (V" = 523.8 ml/min for H = 3 mm and 7 mm; V" = 484.28 ml/min for H = 12 mm) at Different H.

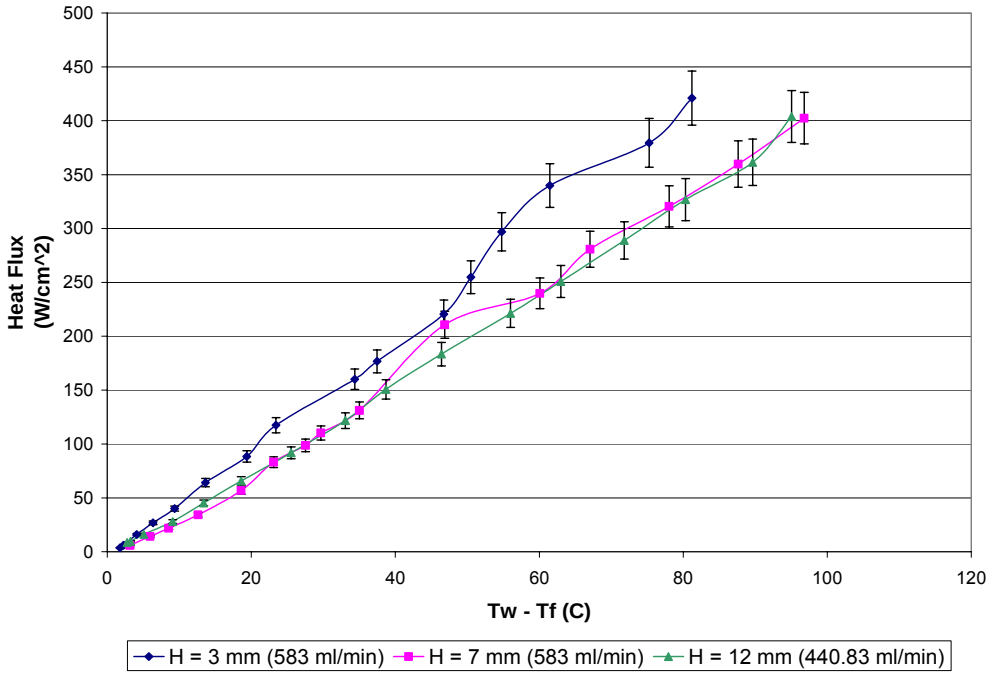

Figure 35: Heat Transfer Curve for P = 25 psi (V" = 583 ml/min for H = 3 mm and 7 mm; V" = 440.83 ml/min for H = 12 mm) at Different H.

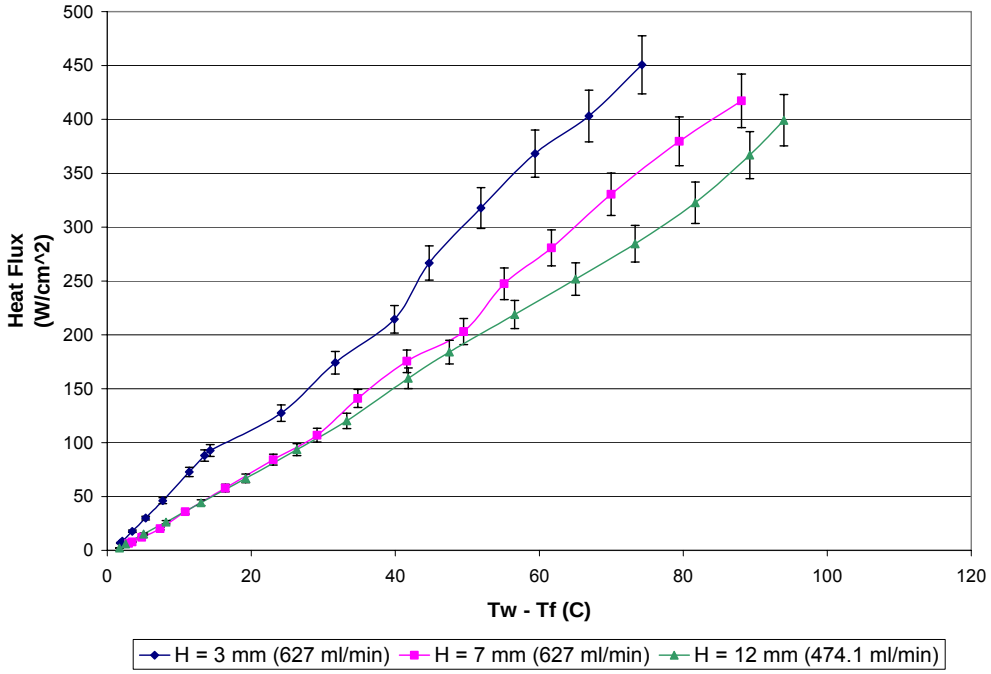

Figure 36: Heat Transfer Curve for P = 30 psi (V" = 627 ml/min for H = 3 mm and 7 mm; V" = 474.1 ml/min for H = 12 mm) at Different H.

Table 7 and Figure 37 show a comparison of the results of this investigation to those of other researchers like Jiang, and Mudawar. Mudawar, I., and Estes, K.A. [33], studied the effect of spray nozzle orifice, volumetric flux, liquid subcooling and working fluids like Fluorinert FC-72, FC-87, and water. The boiling curves presented by Mudawar and Estes show that there is a slight increase in slope of the boiling curves between the single phase and nucleate boiling regimes for high volumetric fluxes.

Table 7: Comparison between Present and Previous Works.

Author	Sato	Jiang [10]	Mudawar [33]
q"(W/cm^2) min-max	1.9 – 451	10 – 110	2-190
G x 10^3 ($ml/s/mm^2$) min-max	54 – 92	3.3	0.6 - 9.96

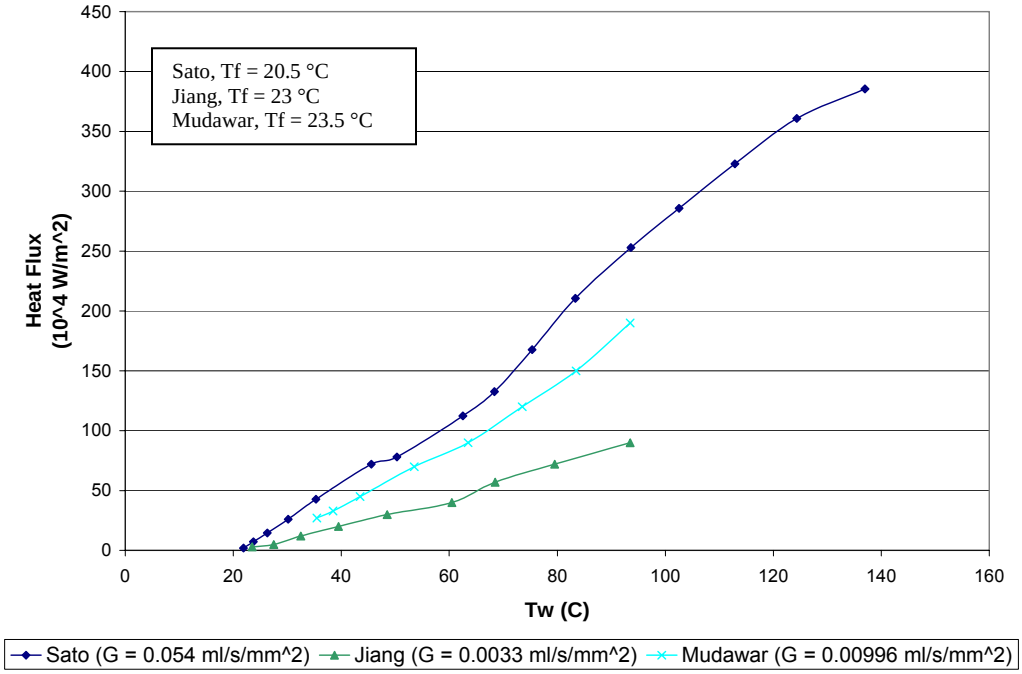

Figure 37: Comparison between Present and Previous Works.

Chapter 4 – Discussion and Conclusion

Heat fluxes between 1.92 to 451 W/cm^2; 2.1 to 417.3 W/cm^2 and 1.9 to 409.5 W/cm^2 were obtained for H = 3, 7 and 12 mm respectively at various input power levels. These high heat fluxes are very similar to heat fluxes obtained by Lin, L. et al [7] near Tw = 100 °C. For a flow rate of 298.8 ml/min and a test surface temperature of 100 °C, Lin obtained a heat flux over 270 W/cm^2; while for the present study with H = 3 mm, volumetric flow rate of 336.6 ml/min, and a test surface temperature of 100 °C, the heat flux was near 276 W/cm^2, which represents a difference of 6 W/cm^2 or less than 2.5%.

Effect of the distance between the test surface and the nozzle: In this study, for low pressure cases, the effect of the distance on the heat flux was insignificant, as shown in Figures 33 and 34. This is because at very small distances, the sprayed area was very small compared with those at larger distances. But at higher pressures, the heat flux was relatively affected by the distance (H). This behavior is due to the fact that at higher distances, part of the fluid did not impinge the test surface, hence there was a decrease in the volumetric flow rate.

Effect of the volumetric flow rate: This parameter affects the heat flux for the three distances but especially for H = 3 mm. In the case of H = 3mm, T_w =

100 °C, and volumetric flow rate range from 336.6 to 627 ml/min, the heat flux varied from 276.3 to 484.5 W/cm^2 respectively; which represents a difference of 208.2 W/cm^2. The effect of the volumetric flow rate decreases when the distance (H) increases, for example for the case of H = 7 mm, T_w = 100 °C, and volumetric flow rate range from 336.6 to 627 ml/min, the heat flux varied from 283.04 to 380 W/cm^2 respectively; which represents a difference of 96.96 W/cm^2. In conclusion, higher heat fluxes can be obtained using higher volumetric flow rates, but this effect is clearly diminished by the distance (H). This conclusion is very similar to many other researchers, even though their volumetric flow rates were lower than those used in the present study. Ortiz, L. & González, J. E. [8] for example obtained a significantly increase of the heat flux for volumetric flow rates ranging 1.48 to 2.91 l/h (24.67 to 48.5 ml/min).

Chapter 5 – Recommendations

The experimental results in this investigation are valid only for the case of single - phase regime due to the fact that it was not possible to increment more the input power into the heater. For future studies, it is very important to design a new apparatus which can reach higher temperatures. An example of an improvement of the apparatus is the material used as a test surface. An Inconel alloy 625 test surface which can held temperatures over 500 °C, could be used instead of a copper test surface.

It is also very important to understand the impact behavior of the droplets to the heated surface for the case of an up - ward facing spray cooling. The impact behavior of a down-ward facing and an up - ward facing spray cooling are not probably the same due to the fact that the gravity would play an important role, especially at high distances and low pressures.

The parameters studied in this investigation (distance (H) and volumetric flow rate) are two of many other parameters that affect the heat flux. These parameters could be studied in a near future; some of them were already studied for the case of down-ward facing spray cooling like: angle of incidence, finishing surface, number of nozzles, Sauter mean diameter, droplet velocity, etc., but they

still need to be studied for up-ward facing and some of them even for lateral facing spray cooling.

References

[1] Hewitt, G. F., Delhaye, J. M., and Zuber, N., 1982, *Multiphase Science and Technology*, McGraw-Hill, United States of America, pp. 4-13.

[2] Shou-Shing Hsieh, Tsung-Cheng Fan, and Huang-Hsui Tsai, 2004, "Spray Cooling Characteristics of Water and R-134a. Part I: Nucleate Boiling," International Journal of Heat and Mass Transfer, 47(26), pp. 5703-5712.

[3] Rybicki, J. R., and Mudawar, I., 2005, "Single-Phase and Two-Phase Cooling Characteristics of Upward-Facing and Downward-Facing Sprays," International Journal of Heat and Mass Transfer, 49(1-2), pp. 5-16.

[4] Mudawar, I., and Estes, K. A., 1996. "Optimizing and Predicting CHF in Spray Cooling of a Square Surface," ASME Journal of Heat and Mass Transfer, 118, pp. 672-679.

[5] Chen, R. H., Chow, L. C., and Navedo, J. E., 2001, "Effects of Spray Characteristics on Critical Heat Flux in Subcooled Water Spray Cooling," International Journal of Heat and Mass Transfer, 45(19), pp. 4033-4043.

[6] Jia, W., and Qiu, H., 2002, "Experimental Investigation of Droplet Dynamics and Heat Transfer in Spray Cooling," Experimental Thermal and Fluid Science, 27(7), pp. 829-838.

[7] Lin, L., and Ponnapan, R., 2003, "Heat Transfer Characteristics of Spray Cooling in a Closed Loop," International Journal of Heat and Mass Transfer, 46(20), pp. 3737-3746.

[8] Ortiz, L., and González, J. E., 1999, "Experiments on Steady-State High Heat Fluxes Using Spray Cooling," Experimental Heat Transfer, 12(3), pp. 215-233.

[9] Horacek, B., Kiger, K. T., and Kim, J., 2004, "Single Nozzle Spray Cooling Heat Transfer Mechanisms," International Journal of Heat and Mass Transfer, 48(8), pp. 1425-1438.

[10] Jiang, S., and Dhir, V. K., 2004, "Spray Cooling in a Closed System with Different Fractions of Non-Condensibles in the Environment," International Journal of Heat and Mass Transfer, 47(25), pp. 5391-5406.

[11] Fabbri, M., and Dhir, V. K., 2005, “Optimized Heat Transfer for High Power Electronic Cooling Using Arrays of Microjets,” ASME Journal of Heat Transfer, 127, pp. 760-769.

[12] Wang, E. N., Santiago, J. G., Goodson, K. E., and Kenny, T. W., 2004, “Microjet Impingement Cooling with Phase Change,” 2004 ASME International Mechanical Engineering Congress and RD&D Expo.

[13] Oh, C. H., Lienhard, J. H., Younis, H. F., Dahbura, R. S., and Michels, D., 1998, “Liquid Jet-Array Cooling Modules for High Heat Fluxes,” AIChE Journal, 44(4), pp. 769-779.

[14] Oliphant, K., Webb, B. W., and McQuay, M. Q., 1998, “An Experimental Comparison of Liquid Jet Array and Spray Impingement Cooling in the Non-Boiling Regime,” Experimental Thermal and Fluid Science, 18(1), pp. 1-10.

[15] Kizito, J. P., Vander Wal, R. L., and Berger, G., 2004, “Spray Cooling Processes for Space Applications,” NASA/CP-2004-213205/Vol2, National Center for Microgravity Research, Nasa Glenn Research Center.

[16] Kandlikar, S. G., and Steinke, M. E., 2001, “Contact Angles of Droplets During Spread and Recoil After Impinging on a Heated Surface,” IchemE Chemical Engineering Research and Design.

[17] Hatta, N., Fujimoto, H., Takuda, H., Kinoshita, K., and Takahashi, O., 1994, “Collision Dynamics of a Water Droplet Impinging on a Rigid Surface Above the Leidenfrost Temperature,” ISIJ International, 35(1), pp. 50-55.

[18] Ueda, T., Enomoto, T., and Kanetsuki, M., 1979, Bull. Jpn. Sci. Mech. Eng., 22, 724.

[19] Wang, E. N., Zhang, L., Jiang, L., Koo, J., Goodson, K., and Kenny, T., 2004, “Micromachined Jet Arrays for Liquid Impingement Cooling of VLSI Chips,” Journal of MicroElectroMechanicalSystems, 13(5), pp. 833-842.

[20] Bash, C. E., Patel, Ch. D., and Sharma, R. K., 2003, “Inkjet Assisted Spray Cooling of Electronics,” ASME. International Electronic Packaging Technical Conference and Exhibition, IPACK2003-35058.

[21] Garimella, S. V., 2001, “Considerations in the Design of Impingement-Cooled Systems,” Proceedings of the SMTA International 2001, pp. 144-150.

[22] Brignoni, L. A., and Garimella, S. V., 2000, “Effects of Nozzle-Inlet Chamfering on Pressure Drop and Heat Transfer in Confined Air Jet Impingement,” International Journal of Heat and Mass Transfer, 43(7), pp.1133-1139.

[23] Brignoni, L. A., and Garimella, S. V., 1999, “Experimental Optimization of Confined Air Jet Impingement on a Pin Fin Heat Sink,” IEEE Trans. Components and Packaging Technologies, 22(3), pp. 300-308.

[24] Brignoni, L. A., and Garimella, S. V., 2000, “Heat Transfer from a Finned Surface in Ducted Air Jet Suction and Impingement,” ASME J. Electronic Packaging, 122(3), pp. 282-285.

[25] Wu, S., Mai, J., Tai, Y. C., and Ho, C. M., 1999, “Micro Heat Exchanger by Using MEMS Impinging Jets,” Proc. 12th Annual International Workshop on Micro Electro Mechanical System, pp. 171-176.

[26] Loureiro, H. M., Panao, M. R. O., and Moreira, A. L. N., 2004, “Simultaneous Measurements of Droplet Characteristics and Surface Thermal Behavior to Study Spray Cooling with Pulsed Sprays,” Proc. 12th Int. Symposium on Applications of Laser Techniques to Fluid Mechanics.

[27] Jia, W., Aguilar, G., Wang, G. X., and Nelson, J. S., 2004, “Heat-Transfer Dynamics During Cryogen Spray Cooling of Substrate at Different Initial Temperatures,” Physics in Medicine and Biology, 49, pp. 5295-5308.

[28] Pikkula, B. M., Torres, J. H., Tunnel, J. W., and Anvari, Bahman., 2001, “Cryogen Spray Cooling: Effects of Droplet Size and Spray Density on Heat Removal,” Lasers in Surgery and Medicine, 28, pp. 103-112.

[29] Pikkula, B. M., Tunnel, J. W., Chang, D. W., and Anvari, B., 2003, “Effects of Droplet Velocity, Diameter, and Film Height on Heat Removal During Cryogen Spray Cooling,” Annals of Biomedical Engineering, 32(8), pp.1131-1140.

[30] Aguilar, G., Vu, H., and Nelson, J. S., 2004, “Influence of Angle Between the Nozzle and Skin Surface on the Heat Flux and Overall Heat Extraction During Cryogen Spray Cooling,” Physics in Medicine and Biology, 49(10), pp. 147-153.

[31] Kim, J. H., You, S. M., and Choi, S. U. S., 2004, “Evaporative Spray Cooling of Plain and Microporous Coated Surfaces,” International Journal of Heat and Mass Transfer, 47(14-16), pp. 3307-3315.

[32] Xishi, W., Guangxuan, L., Weicheng, F., and Dobashi, R., 2003, "Experimental Study on Cooling a Hot Solid Surface with Water Mist," Journal of Fire Sciences, 22(5), pp. 355-366.

[33] Estes, K. A., and Mudawar, I., 1995, "Correlation of Sauter Mean Diameter and Critical Heat Flux for Spray Cooling of Small Surfaces," International Journal of Heat and Mass Transfer, 38(16), pp. 2985-2996.

[34] Incropera, F. P., Dewitt, D. P., Bergman, T. L., and Lavine, A. S., 2005, *Introduction to Heat and Mass Transfer*, John Wiley & Sons, INC. United States of America. pp. 586.

[35] Baehr, H. D., and Stephan, K., 1996, *Heat and Mass Transfer*, Springer, Berlin.

[36] Hewitt, G. F., Delhaye, J. M., and Zuber, N., 1982, *Multiphase Science and Technology*, McGraw-Hill, United States of America, pp. 295.

[37] Shah, V. L., and Sha, W. T., 1978, "Growth of a Sodium Vapor Bubble Rising in the Superheated Liquid," Nuclear Eng. Design, 45(1), pp. 81-91.

[38] Van Stralen, S. J. D., 1968, "The Growth Rate of Vapour Bubbles in Superheated Pure Liquids and in Binary Mixtures, Part II: Experimental Results," International Journal of Heat and Mass Transfer, 11(10), pp. 1491-1512.

[39] Wikipedia, 2006, "Heat Transfer Coefficient," http://en.wikipedia.org/wiki/Heat_transfer_coefficient.

[40] Barry, B. A., 1978, *Errors in Practical Measurement in Science, Engineering, and Technology*, John Wiley & Sons, INC. Canada. pp. 10-14.

[41] Beauford, J., 1992, *Statistics in Science*, R & E Publishers. United states of America. pp. 6-14.

[42] Wang, G. X., Aguilar, G., and Nelson, J. S., 2003, "Dynamic Behavior of Cryogen Spray Cooling: Effect of Spray Distance," Lasers in Surgery and Medicine, 32, pp. 152-159.

[43] JAHM Software, Inc., 2003, *Material Properties Database* , North Reading, MA.

[44] Incropera, F. P., Dewitt, D. P., Bergman, T. L., and Lavine, A. S., 2005, *Fundamentals of Heat and Mass Transfer*, John Wiley & Sons, INC. United States of America. pp. 62.

Bibliography

Baehr, H. D., and Stephan, K., 1998, *Heat and Mass Transfer,* Springer-Verlag Berlin Heidelberg, Germany.

Barry, B. A., 1978, *Errors in Practical Measurement in Science, Engineering, and Technology,* John Wiley & Sons, Inc., Canada.

Beauford, J., 1992, *Statistics in Science*, R & E Publishers, United states of America.

Hewitt, G. F., Delhaye, J. M., and Zuber, N., 1982, *Multiphase Science and Technology,* Hemisphere Publishing Corporation, United States of America.

Hewitt, G. F., Shires, G. L., and Bott, T. R., 1994, *Process Heat Transfer,* CRC Press, Inc., United States of America.

Kraus, A. D., Aziz, A., and Welty, J., 2001, *Extended Surface Heat Transfer,* John Wiley & Sons, Inc., Canada.

Mills, A. F., 1995, *Heat and Mass Transfer,* Richard D. Irwin, INC., United States of America.

Rabinovich, S., 1993, *Measurement Errors: Theory and Practice,* American Institute of Physics, United States of America.

Appendices

Appendix A: Heat Flux and Temperature of Surface Calculation

The temperatures in points (1), (2) and (3) were:

- $TC_{1,m}$ = 87.65 °C.
- $TC_{2,m}$ = 128.74 °C.
- $TC_{3,m}$ = 166.12 °C.

Then the heat flux along points (1)-(2) can be calculated as:

$$q''_{1-2} = 400\ W/mK \times \frac{(128.74 - 87.65)}{0.01m} = 1643600\ W/m^2$$

The same with points (2)-(3):

$$q''_{2-3} = 400\ W/mK \times \frac{(166.12 - 128.74)}{0.01m} = 1495200\ W/m^2$$

Then the heat flux between the heated surface and point (1) can be calculated using equation (4):

$$q''_{w-1} = 1643600 + \frac{13 \times (1643600 - 1495200)}{20} = 1740060\ W/m^2$$

The temperature of the heated surface can be obtained from the calculated heat flux, using equation (5):

$$T_w = 87.65\ °C - \frac{0.003\ m \times 1740060\ W/m^2}{400\ W/mK} = 74.6\ °C$$

Table 8: Heat Flux and Temperature of the Heated Surface for H = 3 mm.

Input Power (W)	V" = 336.6 ml/min		V" = 464.6 ml/min		V" = 523.8 ml/min		V" = 583 ml/min		V" = 627 ml/min	
	Tsurf (°C)	Heat flux (W/m^2K)	Tsurf (°C)	Heat flux (W/m^2K)	Tsurf (°C)	Heat flux (W/m^2K)	Tsurf (°C)	Heat flux (W/m^2K)	Tsurf (°C)	Heat flux (W/m^2K)
1.5	21.89	19213	22.29	41014.12	22.2	38344	22.27	37179.68	22.33	69714.16
7.2	23.72	71570.4	22.93	62805.2	23.6	76822	22.76	60410	22.6	85798.4
19.9	26.31	145943.76	25.29	154476.2	25.77	207524.24	24.61	160522.32	23.99	177493.52
37.7	30.18	260738.08	28.86	256584.12	28.83	287281.8	26.87	268968.8	25.83	300343.28
63.1	35.32	426793.92	32.92	447721.08	32.63	420324.84	29.86	401286.32	28.2	462035.08
92.6	45.57	720741.8	38.1	606586.96	40.23	620974.8	34.15	642257.84	31.89	728515
122.6	50.32	780181.44	43.92	878349.8	42.94	826108.56	39.88	884540.88	34.01	880433.12
163.5	62.54	1123225.32	49.93	1139029.24	47.48	1167232.24	43.94	1174559.68	34.8	927684.36
202.7	68.37	1326443.16	59.22	1456557.44	52.86	1501833.96	54.88	1601187.52	44.67	1274480
247.2	75.35	1677236.68	66.15	1655300.88	61.41	1872365.04	57.98	1767223.64	52.16	1742160
296	83.35	2105760.76	71.5	2103209.04	66.12	2203171.68	67.24	2205062.08	60.39	2144920
359.2	93.64	2529772.36	80.29	2431119.6	72.44	2550210.56	71.01	2548466.28	65.22	2667340
416.7	102.56	2857340.28	87.7	2854858.28	83.85	2892233.12	75.29	2969995.04	72.39	3178180
491	112.91	3229739.08	105.02	3028784.52	90.38	3336728.92	81.96	3398593.96	79.9	3682940
557.4	124.35	3608324.48	117.32	3438969.24	97.21	3761921.48	95.76	3795441.04	87.41	4031780
628.6	136.98	3854440	130.89	3795765.6	107.85	4079969.96	101.7	4210666.2	94.76	4506780

Table 9: Heat Flux and Temperature of the Heated Surface for H = 7 mm.

Input Power (W)	V" = 336.6 ml/min		V" = 464.6 ml/min		V" = 523.8 ml/min		V" = 583 ml/min		V" = 627 ml/min	
	Tsurf (°C)	Heat flux (W/m^2K)	Tsurf (°C)	Heat flux (W/m^2K)	Tsurf (°C)	Heat flux (W/m^2K)	Tsurf (°C)	Heat flux (W/m^2K)	Tsurf (°C)	Heat flux (W/m^2K)
1.5	21.89	19213	22.29	41014.12	22.2	38344	22.27	37179.68	22.33	69714.16
7.2	23.72	71570.4	22.93	62805.2	23.6	76822	22.76	60410	22.6	85798.4
19.9	26.31	145943.76	25.29	154476.2	25.77	207524.24	24.61	160522.32	23.99	177493.52
37.7	30.18	260738.08	28.86	256584.12	28.83	287281.8	26.87	268968.8	25.83	300343.28
63.1	35.32	426793.92	32.92	447721.08	32.63	420324.84	29.86	401286.32	28.2	462035.08
92.6	45.57	720741.8	38.1	606586.96	40.23	620974.8	34.15	642257.84	31.89	728515
122.6	50.32	780181.44	43.92	878349.8	42.94	826108.56	39.88	884540.88	34.01	880433.12
163.5	62.54	1123225.32	49.93	1139029.24	47.48	1167232.24	43.94	1174559.68	34.8	927684.36
202.7	68.37	1326443.16	59.22	1456557.44	52.86	1501833.96	54.88	1601187.52	44.67	1274480
247.2	75.35	1677236.68	66.15	1655300.88	61.41	1872365.04	57.98	1767223.64	52.16	1742160
296	83.35	2105760.76	71.5	2103209.04	66.12	2203171.68	67.24	2205062.08	60.39	2144920
359.2	93.64	2529772.36	80.29	2431119.6	72.44	2550210.56	71.01	2548466.28	65.22	2667340
416.7	102.56	2857340.28	87.7	2854858.28	83.85	2892233.12	75.29	2969995.04	72.39	3178180
491	112.91	3229739.08	105.02	3028784.52	90.38	3336728.92	81.96	3398593.96	79.9	3682940
557.4	124.35	3608324.48	117.32	3438969.24	97.21	3761921.48	95.76	3795441.04	87.41	4031780
628.6	136.98	3854440	130.89	3795765.6	107.85	4079969.96	101.7	4210666.2	94.76	4506780

Table 10: Heat Flux and Temperature of the Heated Surface for H = 12 mm.

Input Power (W)	V" = 336.6 ml/min		V" = 464.6 ml/min		V" = 523.8 ml/min		V" = 583 ml/min		V" = 627 ml/min	
	Tsurf (°C)	Heat flux (W/m^2K)	Tsurf (°C)	Heat flux (W/m^2K)	Tsurf (°C)	Heat flux (W/m^2K)	Tsurf (°C)	Heat flux (W/m^2K)	Tsurf (°C)	Heat flux (W/m^2K)
1.5	21.89	19213	22.29	41014.12	22.2	38344	22.27	37179.68	22.33	69714.16
7.2	23.72	71570.4	22.93	62805.2	23.6	76822	22.76	60410	22.6	85798.4
19.9	26.31	145943.76	25.29	154476.2	25.77	207524.24	24.61	160522.32	23.99	177493.52
37.7	30.18	260738.08	28.86	256584.12	28.83	287281.8	26.87	268968.8	25.83	300343.28
63.1	35.32	426793.92	32.92	447721.08	32.63	420324.84	29.86	401286.32	28.2	462035.08
92.6	45.57	720741.8	38.1	606586.96	40.23	620974.8	34.15	642257.84	31.89	728515
122.6	50.32	780181.44	43.92	878349.8	42.94	826108.56	39.88	884540.88	34.01	880433.12
163.5	62.54	1123225.32	49.93	1139029.24	47.48	1167232.24	43.94	1174559.68	34.8	927684.36
202.7	68.37	1326443.16	59.22	1456557.44	52.86	1501833.96	54.88	1601187.52	44.67	1274480
247.2	75.35	1677236.68	66.15	1655300.88	61.41	1872365.04	57.98	1767223.64	52.16	1742160
296	83.35	2105760.76	71.5	2103209.04	66.12	2203171.68	67.24	2205062.08	60.39	2144920
359.2	93.64	2529772.36	80.29	2431119.6	72.44	2550210.56	71.01	2548466.28	65.22	2667340
416.7	102.56	2857340.28	87.7	2854858.28	83.85	2892233.12	75.29	2969995.04	72.39	3178180
491	112.91	3229739.08	105.02	3028784.52	90.38	3336728.92	81.96	3398593.96	79.9	3682940
557.4	124.35	3608324.48	117.32	3438969.24	97.21	3761921.48	95.76	3795441.04	87.41	4031780
628.6	136.98	3854440	130.89	3795765.6	107.85	4079969.96	101.7	4210666.2	94.76	4506780

Appendix C: Heat Transfer Coefficient Calculation

As an example of calculation, data from experiments with H = 3 mm, V" = 336.6 ml/min, and IP = 163.5 W were used:

- q" = 1123225.32 W/m^2
- T_w = 62.54 °C.

Using equation (8), the heat transfer coefficient was:

$$h = \frac{1123225.32}{(62.54-20.5)} = 26718.01\ W/m^2K$$

Table 11: Heat Transfer Coefficient for H = 3 mm.

Input Power (W)	V" = 336.6 ml/min h (W/m^2K)	V" = 464.6 ml/min h (W/m^2K)	V" = 523.8 ml/min h (W/m^2K)	V" = 583 ml/min h (W/m^2K)	V" = 627 ml/min h (W/m^2K)
1.5	13822.30	22912.92	22555.29	21005.47	38095.17
7.2	22226.83	25845.76	24781.29	26730.09	40856.38
19.9	25119.41	32249.73	39378.41	39056.53	50857.74
37.7	26935.75	30691.88	34487.61	42224.30	56349.58
63.1	28798.51	36048.40	34651.68	42872.47	60004.56
92.6	28749.17	34465.17	31473.63	47051.86	63960.93
122.6	26163.03	37504.26	36814.11	45641.94	65168.99
163.5	26718.01	38703.00	43262.87	50109.20	64873.03
202.7	27709.28	37617.70	46410.20	46573.23	52729.83
247.2	30578.61	36260.70	45767.91	47151.11	55027.16
296	33504.55	41239.39	48293.99	47177.19	53770.87
359.2	34588.08	40660.97	49099.16	50454.69	59645.35
416.7	34820.14	42483.01	45654.82	54206.88	61248.41
491	34950.10	35835.12	47749.41	55297.66	62002.36
557.4	34745.54	35519.20	49040.82	50431.05	60256.76
628.6	33091.00	34385.05	46708.30	51855.50	60689.20

Table 12: Heat Transfer Coefficient for H = 7 mm.

Input Power (W)	V" = 336.6 ml/min h (W/m^2K)	V" = 464.6 ml/min h (W/m^2K)	V" = 523.8 ml/min h (W/m^2K)	V" = 583 ml/min h (W/m^2K)	V" = 627 ml/min h (W/m^2K)
1.5	21565.28	8825.23	18907.97	18978.15	22761.16
7.2	21732.12	15051.11	21139.54	18942.48	21733.91
19.9	23557.63	18860.39	24936.37	23926.12	25509.25
37.7	24857.83	21044.45	26169.05	25724.43	27487.53
63.1	27552.14	23003.56	30761.00	27072.16	33172.81
92.6	26320.44	23823.22	29455.01	30513.51	35324.18
122.6	29392.10	25809.81	32085.44	35962.50	36507.90
163.5	29965.22	26576.76	32082.01	35875.29	36711.87
202.7	28870.98	31600.83	34652.27	37154.97	40545.91
247.2	32156.97	33956.27	35042.52	37470.30	42193.21
296	33716.00	35193.13	41434.91	44973.59	41028.19
359.2	35446.15	32319.89	36731.25	39906.63	44895.63
416.7	35643.66	35912.29	33375.94	41860.26	45516.06
491	37393.21	37598.84	38463.16	41074.18	47229.27
557.4	35623.63	38548.66	37997.77	41071.87	47801.99
628.6	35690.94	38192.35	38832.21	41583.26	47371.67

Table 13: Heat Transfer Coefficient for H = 12 mm.

Input Power (%)	V" = 336.6 ml/min h (W/m^2K)	V" = 440.83 ml/min h (W/m^2K)	V" = 464.6 ml/min h (W/m^2K)	V" = 474.1 ml/min h (W/m^2K)	V" = 484.28 ml/min h (W/m^2K)
1.5	29600.74	30906.53	12612.55	13342.56	13666.43
7.2	27415.60	30130.53	20132.71	23220.94	24460.12
19.9	10108.56	31892.84	29339.44	30135.94	30413.97
37.7	23597.42	30860.86	32275.50	32063.79	33287.20
63.1	21030.21	33787.62	34419.51	34027.22	34979.82
92.6	26461.89	35319.32	35511.54	34758.30	36046.44
122.6	25224.10	35956.05	36483.22	35519.49	36961.91
163.5	26055.84	36822.90	37756.45	36140.46	37993.01
202.7	27885.76	38956.30	38845.06	38223.59	39147.28
247.2	29711.96	39533.30	39727.37	38740.15	40746.97
296	31520.33	39516.26	41031.28	38684.05	40767.79
359.2	34613.51	39814.51	40221.56	38718.96	40843.12
416.7	34946.16	40247.30	40445.73	38831.06	41177.04
491	34861.77	40701.51	40782.39	39500.02	41756.44
557.4	36710.64	40331.58	41684.18	41124.14	42780.57
628.6	35118.29	42493.07	42613.08	42495.31	43153.70

Appendix E: Volumetric Flow Rate Calculation

As an example of calculation, a distance H = 12 mm and P = 25 psi were used. Other parameters used were area of the test surface (A_w), and sprayed area (A_{spray}) :

- A_w = 113.1 mm^2 (using Φ = 12 mm, see subchapter 3.4.2).
- A_{spray} = 149.6 mm^2 (using W/H = 1.15 and H = 12 mm, see subchapter 3.4.2).

The total volumetric flow rate was measured using a flowmeter. For the case of P = 25 psi, $V"_T$ was 583 ml/min (see Table 2, from subchapter 3.4.2). Then, the volumetric flow rate in the test surface was calculated using the following formula:

$$V" = V"_T \times \frac{A_w}{A_{spray}}$$

$$\rightarrow V" = 440.83 \text{ ml/min}$$